Description of the Neoselachii material from the Early Triassic Grippia level Bonebed of Spitsbergen, Norway

Synnøve Mo Saugen

Master Thesis
Sedimentology, Paleontology and Stratigraphy
60 credits

Department of Geosciences
Faculty of Mathematics and Natural Sciences

Natural History Museum
UNIVERSITY OF OSLO

May 2022

Description of the Neoselachii material from the Early Triassic Grippia level Bonebed of Spitsbergen, Norway

Synnøve Mo Saugen

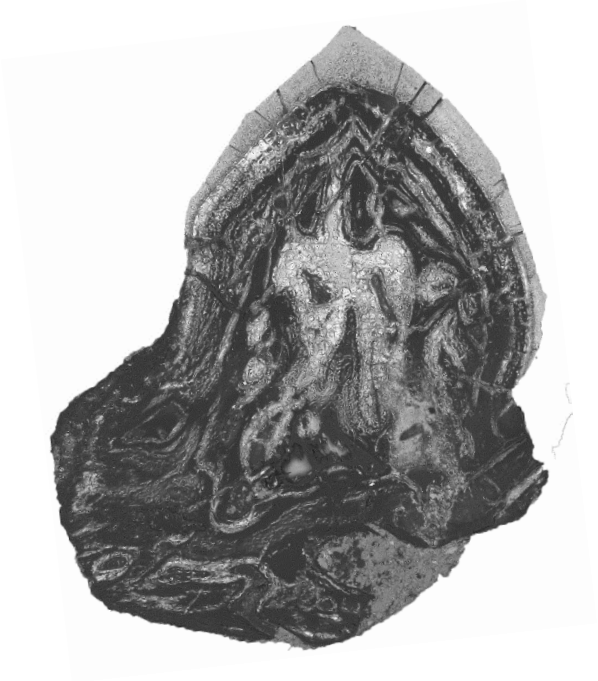

Master Thesis
Sedimentology, Paleontology and Stratigraphy
60 credits

Department of Geosciences
Faculty of Mathematics and Natural Sciences

Natural History Museum
UNIVERSITY OF OSLO

May 2022

2022

Description of the Neoselachii material from the Early Triassic Grippia level Bonebed of Spitsbergen, Norway

Synnøve Mo Saugen

http://www.duo.uio.no/

Trykk: Reprosentralen, Universitetet i Oslo

Abstract

Five new neoselachians from the Early Triassic of Spitsbergen are here described; *Synechodus* sp., *Synechodus incrementum*, *Rhomphaiodon minor*, *Rhomphaiodon nicolensis* and *Grozonodon* sp. An abundant amount of shark teeth from the Grippia level Bonebed have been collected, sorted and described. The teeth were studied using various methods, including thin sections, SEM- and CT-imaging. With this new material, the taxonomic position of *S. incrementum* within Synechodontiformes (Neoselachii) is proved. Two new species of neoselachians, *Synechodus* sp. and *Grozonodon* sp., are described for the first time. This thesis gives proof of an earlier development of the neoselachian triple-layered enameloid, as well as serrated cutting edges, than previously thought. Additionally, the thesis discusses the uncertainties within species determination based on isolated teeth, and compares the different methods used to study the material.

Acknowledgement

Since I was a little kid, I have always been fascinated by the Earth's history and the life that has been. Sharks have been a special interest of mine because they have been around for hundreds of millions of years, and they are now endangered by extinction. I am truly grateful for getting the opportunity to study my master here at the Natural History Museum of Oslo, about this subject that I really care about.

First, I want to direct the biggest thank you to my main supervisor Jørn H. Hurum, for always taking the time to answer all my big and small questions and giving me helpful feedback. I also want to thank my supervisors Aubrey J. Roberts and Victoria S. Engelschiøn for your great workshops and for taking time off your maternity leave for following-up and feedback. Thanks to Hans Arne Nakrem for showing me everything about photographing and photo editing. Thank you to Øyvind Hammer for taking the CT-scans for me. Thank you Salahalldin Akhavan for making the amazing thin sections. Also, thank you to Nélia Castro and Siri Simonsen for teaching me how to use the SEM.

I want to thank my fellow students at Økern, Maren K. Stokke, Mees F. Auener, Audun Rugstad and Karoline H. Aasberg, for a great study environment, proofreading and taking highly needed coffee-, ice cream- and board game breaks. Together with the rest of the people at Økern for contributing to a nice work environment.

And last, thank you to friends and family for supporting and motivating me to write this thesis, and in general for being interested in listening to my never-ending monologues about sharks.

I am greatly appreciative of every single one of you.

- *Synnøve M. Saugen, Oslo, May 2022.*

Table of contents

1. Introduction

1.1 Mass extinction events

Species go extinct all the time. When this normal extinction rate does not impact the biodiversity on a broad scale it is called *background extinction*. A mass extinction event is defined as when the extinction rate is considerably higher than the background extinction, is wide geographically spread and happens within a short geological time frame (Raup and Sepkoski, 1982).

Throughout Earth's history five big mass extinction events have taken place, commonly referred to as "the big five", occurring in the End Ordovician, End Devonian, End Permian, End Triassic and End Cretaceous (Sepkoski, 1986). The most fatal of them being in the End Permian (Scheyer et al., 2014), also called the Permian-Triassic Mass Extinction (PTME), with a total of 62% extinction at genus level (Stanley, 2016).

In addition to "the big five" it has been suggested that we are now entering a sixth mass extinction event (Barnosky et al., 2011; Ceballos et al., 2015; Ceballos et al., 2017; Ceballos et al., 2020). Ceballos et al. (2020) state that humans are responsible for this mass extinction, both in terms of elevated greenhouse gas emissions, but also due to habitat loss related to modern agriculture (Tilman et al., 2017; Williams et al., 2021).

This thesis will describe a major new collection of shark teeth from the early recovery after the PTME. Understanding how previous mass extinctions affected the environment can help with understanding the ongoing events.

1.1.1 The Permian-Triassic Mass Extinction

The Permian-Triassic Mass Extinction occurred at the end of the Permian, around 252 million years ago (Cohen et al., 2013). The cause of PTME is complex. During the end of the Permian the global temperature increased (Joachimski et al., 2012). Volcanism related to the Siberian Traps, a large area of volcanic rocks in Siberia of Russia, caused the atmospheric concentration of carbon dioxide to increase (Vázquez and Clapham, 2017), contributing to the global warming (Burgess et al., 2017). Wignall and Twitchett (1996) suggest that marine biota was affected by

ocean anoxia. Together with anoxia, a loss of habitat in the marine realm occurred associated with the extensive regression of the End Permian (Song et al., 2013; Yin et al., 2014; Li et al., 2021).

The greenhouse gases emitted in relation to the Siberian Traps were not the only cause of the global warming. Wu et al. (2021) state that along with the volcanic emission, methane and carbon dioxide emitted from organic matter played a role as well. Temperatures in the equatorial oceans may have been as high as 40°C, causing marine fauna to migrate towards the poles (Bernardi et al., 2018). According to Raup (1979), as much as 96% of marine species may have gone extinct. However, Stanley (2016) states that it was *only* 81% of marine species. This number considers cluster losses and subtracts background extinction from total extinction. He also rejects the statement that life nearly died out at the End Permian.

The marine fauna was not the only one suffering through the PTME. While the tropic oceans had extreme temperatures, temperatures on land may have been even higher (Bernardi et al., 2018). The interval between the paleolatitudes 15°N and 31°S in the Early Triassic is called the "death belt", due to the lack of terrestrial tetrapods (Romano et al., 2020).

The Permian-Triassic Mass Extinction happened over two episodes: one in the End Permian and one in the Early Triassic. The event happened over a total of 13 million years (Yin and Song, 2013). The first episode resulted in 57% of marine species becoming extinct, affecting the non-motile organisms in the photic zone (e.g. algae, corals and sponges) the most (Yin and Song, 2013). The second episode, in the Early Triassic, resulted in the extinction of 71% of the remaining marine species. This episode also changed the marine ecosystem completely, from being dominated by non-motile species to being dominated by motile species (Song et al., 2013). Volcanism related to the integration of Pangea was most likely the dominant cause for the first episode (Yin and Song, 2013), while the second episode was heavily affected by anoxia (Li et al., 2021).

1.2 Class Chondrichthyes

Chondrichthyes can be divided into two major subclasses, Elasmobranchii and Holocephali (Boisvert et al., 2019), respectively including true sharks and rays (Klug, 2010), and chimeras (Lund and Grogan, 1997). A synapomorphy for Chondrichthyes is their cartilaginous skeleton

(Dean and Summers, 2006; Brazeau and Friedman, 2014). Due to the cartilaginous skeleton, whole specimens are a rare find. However, chondrichthyans shed their teeth often, and there is therefore a rich dental fossil record (Heinicke et al., 2009).

Chondrichthyans first appeared in the Silurian (Zhu et al., 2009; Brazeau and Friedman, 2015; Dearden et al., 2021). However, Chondrichthyan-like scales of Mongolepidida indicate that it could be as early as the Ordovician (Figure 1) (Andreev et al., 2015; Andreev et al., 2016; Boisvert et al., 2019; Manzanares Ubeda, 2020).

The early branching of gnathostomes (jawed vertebrates) into Osteichthyes (bony fishes and tetrapods) and Chondrichthyes (cartilaginous fishes), and the phylogenetic placement of acanthodians (spiny sharks) have for a long time been under debate. The controversy comes from that acanthodians share features with both bony- and cartilaginous fishes. Recent studies prove that acanthodians are stem-chondrichthyans (Coates et al., 2018; Dearden et al., 2021; Maisey et al., 2021; Rücklin et al., 2021). This means that the chondrichthyan lineage dates further back than the previous common consensus of the Devonian, where the first body fossil of a crown-chondrichthyan is described (Miller et al., 2003).

Neoselachians are a group that includes all living true sharks and rays, and their extinct ancestors (Figure 1) (Underwood, 2006). Neoselachians have stronger vertebrae than earlier chondrichthyans, allowing them to become faster swimmers (Cuny and Benton, 1999). They also developed more flexible jaws, better manoeuvrability and an improved sensory system, all of this made them better predators (Benton, 1987). Synechodontiformes represents the earliest order of neoselachian sharks (Klug and Kriwet, 2008), and was one of the more diverse groups of the Jurassic (Klug, 2009). These stem-neoselachians are believed to have given rise to the extant Hexanchiformes (Selachimorpha), the frilled sharks and the cow sharks (Duffin and Ward, 1993).

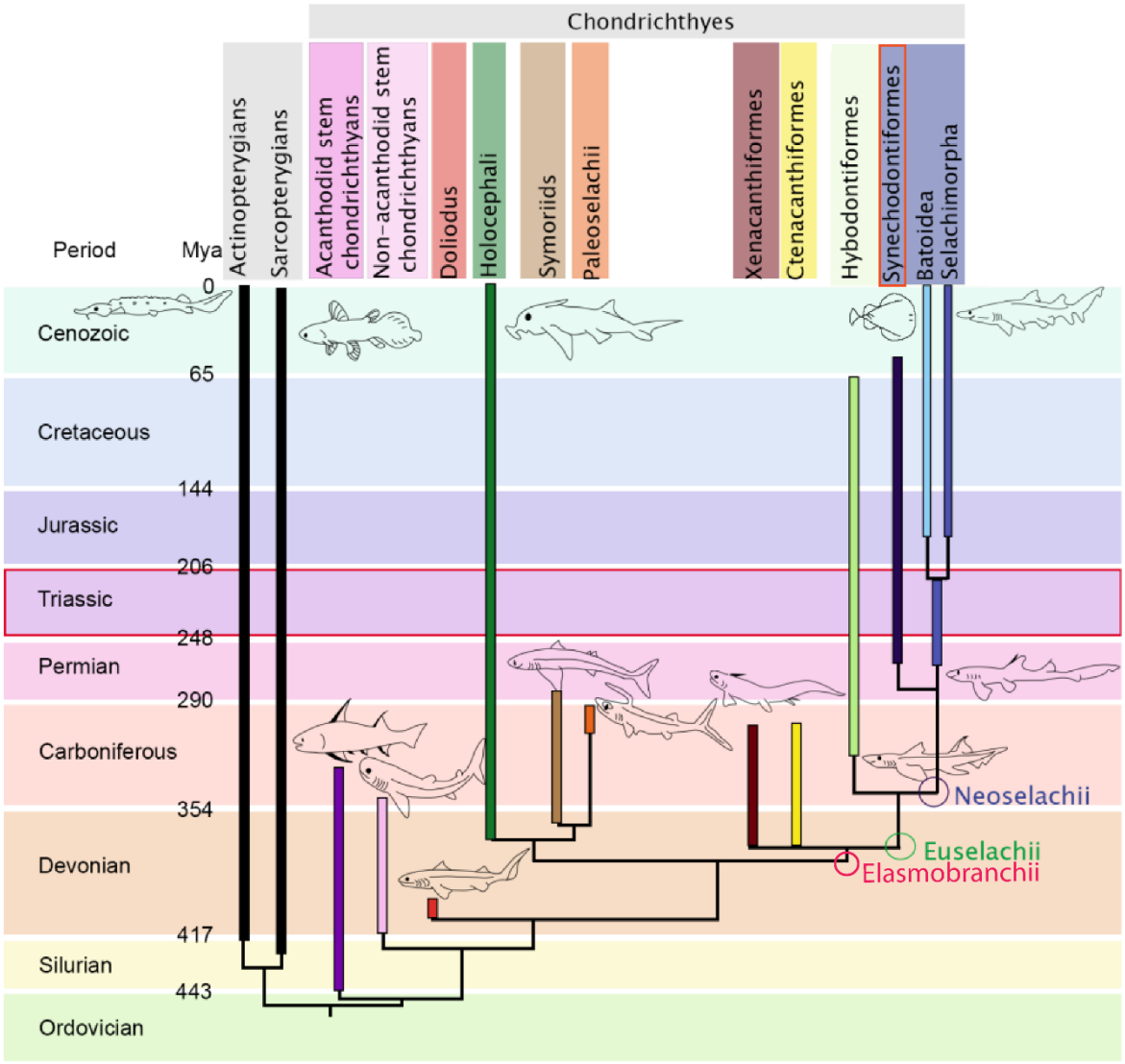

Figure 1 - Phylogeny, appearance and extinction of chondrichthyan groups. Here acanthodians are considered stem-chondrichthyans. Triassic and Synechodontiformes are outlined due to the relevance of this study. Modified from Manzanares Ubeda (2020).

1.2.1 Chondrichthyans after PTME

The chondrichthyans surviving the PTME include the groups Hybodontiformes, Neoselachii and Holocephali (Boisvert et al., 2019; Manzanares Ubeda, 2020) (Figure 1). However, Koot (2013) and Guinot et al. (2013) include Xenacanthiformes as survivors of the PTME. In the Triassic and Jurassic Hybodontiformes was the dominant group. They became extinct when the neoselachians displaced them in the Cretaceous (Carrillo-Briceño et al., 2016).

Chondrichthyans represent the top predators, together with the marine tetrapods, of the Early Triassic marine fauna (Scheyer et al., 2014). Hybodontiformes, the dominant group of the Triassic, shows great diversity. From apex-predators with tearing dentition (Bratvold et. al 2018), to durophagous sharks with grinding teeth (Romano et. al 2019).

Although the phylogenetic relationships within the order Synechodontiformes are uncertain, Klug (2010) concluded that Synechodontiformes is a monophyletic group. Today, 11 genera have been assigned to the order Synechodontiformes, five of which existed in the Triassic. *Safrodus,* described by Koot et al. (2015) from the Lower Triassic of Oman; *Rhomphaiodon,* described from the Upper Triassic of England and France by Cuny and Risnes (2005); *Synechodus,* described by Cuny and Risnes (2005) from the Upper Triassic of England and Belgium, and by Yamagishi (2004) from the Lower/Middle Triassic of South-West Japan, also from the Upper Triassic of British Columbia by Johns et al. (1997); *Mucrovenator,* described by Cuny et al. (2001) from the Middle Triassic of Nevada; *Nemacanthus,* fin spine described by Bratvold et al. (2018) and by Stensiö (1921) from the Lower Triassic of Svalbard and by Romano et al. (2019) from the Lower Triassic of Idaho.

The reason behind the success of chondrichthyans can be explained by multiple factors. Hybodontiform sharks evolved a high capability to osmoregulate, allowing them to live in euryhaline environments and thereby surviving in the coastal areas that were not as affected by ocean anoxia (Vázquez and Clapham, 2017). This advanced osmoregulation also made them more resistant to acidic conditions (Vázquez and Clapham, 2017). Also, the body size of chondrichthyans is negatively correlated to population growth size (Hutchings et al., 2012), meaning that a smaller shark would have a better chance of not going extinct. Chondrichthyan success after the PTME may be due to their reduction in body size in the Triassic, along with having short lifespans and evolving oviparity (Kriwet et al., 2009).

1.2.2 The history of Triassic chondrichthyans of Svalbard

Chondrichthyans have been studied at Svalbard for the past 150 years. Hulke (1873) was the first to describe Triassic fishes from Svalbard. Among these was a shark belonging to the Family Hybodontidae – *Acrodus spitzbergensis.* The material was collected by Nordenskiöld on his expeditions in 1864 and 1868.

Stensiö (1918) described *Hybodus* sp., *Acrodus spitzbergensis?, Acrolepis arctica?* and *Gyrolepis?* sp. Based on material collected in Hornsund. Stensiö (1921) described 11 species, nine of them which were not previously described, in his work on *Triassic fishes from Spitzbergen.* The material was collected over several small expeditions in the time frame from 1912 to 1918, in the Isfjorden area.

Cox and Smith (1973) described a hybodont cephalic spine and a tooth belonging to *Acrodus* from the material gathered by the Cambridge Spitsbergen Expedition in the Lower Triassic, Vikinghøgda Formation of Marmierfjellet.

During the Polish Spitsbergen Expedition of 1960 fish material was collected from the Lower Triassic, Vardebukta Formation in Hornsund, South Spitsbergen (Birkenmajer and Jerzmańska, 1979). Four hybodonts were identified by Birkenmajer and Jerzmańska (1979): *Hybodus sassiensis, Hybodus microdus, Acrodus spitzbergensis, Polyacrodus angulatus* as well as fragments of Holocephali teeth.

Multiple polish expeditions were organized in the Hornsund area. Błażejowski (2004) described the material excavated during the Polish Spitsbergen Expedition of 1998 from the Vardebukta Formation. The material described includes teeth of five hybodont sharks: *Lissodus angulatus, Acrodus spitzbergensis, Hybodus microdus, Hybodus sassiensis* and *Hybodus* sp.

A more complete specimen of *Palaeobates polaris* was described from the Vikinghøgda Formation, "Fish Horizon" at Steinsiöfjellet, by Romano and Brinkmann (2010). The material was gathered on the Swiss-Norwegian expedition of 2008 and includes a part of the mandible, with remaining dentition and labial cartilage; dentition from the upper jaw; part of the hyoid arch; fin spine fragment; parts of the shoulder girdle; pectoral fin; anterior dorsal fin; basal- and radial cartilages and dermal denticles.

From the material collected by Spitsbergen Mesozoic Research Group in 2015, 15 species were described by Bratvold et al. (2018). This material belongs to the Vikinghøgda Formation, Grippia level Bonebed, of Marmierfjellet. A total of 552 teeth, three fin spines and one cephalic spine were identified. Amongst the hybodont sharks were species belonging to genus *Acrodus, Hybodus, Polyacrodus, Palaeobates* and *Lissodus.* In addition to the hybodonts, Bratvold et al. (2018) described two different species of neoselachian sharks based on tooth morphology. They belong to the order Synechodontiformes. Bratvold et al. (2018) also described a third

synechodontiform, *Nemacanthus*, based on fin spine material. There has only been one discovery of neoselachians at Svalbard before Bratvold et al. (2018), that being *Nemacanthus* fin spines (Stensiö, 1921; Koot, 2013). Stensiö (1921) described a selachian fin spine, which Koot (2013) later identified as *Nemacanthus*.

This study aims to identify and describe the new synechodontiform teeth from the Lower Triassic of Svalbard mentioned by Bratvold et al. (2018), but not described in detail. Additional material has later been retrieved, and this will be useful in determining the Synechodontiformes from Bratvold et al. (2018). Bratvold et al. (2018) suggested the material represented at least one new taxon. This master will examine the new Neoselachii material and decide whether these can be referred to a known genus or species, or if they represent a new taxon.

During the extensive period of studying Triassic chondrichthyans of Svalbard, neoselachians have not been described in detail. The only known Neoselachii genus is *Nemacanthus*. This master thesis will take a deep dive into the Triassic neoselachians of Svalbard. With the new material this thesis aims to answer:

1. What did the Neoselachii fauna of Spitsbergen look like during the recovery after PTME?

2. How can this description of Early Triassic neoselachians of Spitsbergen give new insight to the early evolution of neoselachians?

2. Material and Methods

2.1 Material

For this project, an estimate of around 6000 shark teeth and fragmented shark teeth were examined and sorted. 360 teeth were picked out for further examination. Out of these 360, 23 representative teeth were picked out for further histological studies.

The material was gathered during the excavation of 2016 by the Spitsbergen Mesozoic Research Group (SMRG) where 27 m^2 from the Grippia level Bonebed of Marmierfjellet were recovered.

2.1.1 The Bonebed - Geological setting

In the Early Triassic the area was situated in an embayment on the northern margin of Pangaea, at 45 degrees paleolatitude (Hurum et al., 2018).

All teeth described in this study are found in the Grippia Bonebed at Marmierfjellet. Buchan et al. (1965) were the first to present a scheme of the Triassic stratigraphy of Svalbard. Based on Buchan's work, Mørk et al. (1999) defined the Vikinghøgda Formation. Hansen et al. (2018) presented a detailed description of the stratigraphy of the Lower Triassic and determined the age of the Grippia niveau Bonebed located in Vendomdalen Member of the Vikinghøgda Formation (Figure 2).

The Vikinghøgda Formation of Svalbard consists of the Lustaniadalen Member and the Vendomdalen Member and is characterized by an upward fining succession, from sandy siltstone to silty grey shale and black shale. Dolomitic and calcitic cementations are found throughout the formation. The formation was deposited in a shallow marine environment. A rising sea level is prominent from an observed decrease in grain size and an increase of organic matter.

Vendomdalen Member is in the upmost part of the Vikinghøgda Formation, right underneath the Botnheia Formation. The boundary between the Lustaniadalen Member and the Vendomdalen Member lies on top of a yellow sandstone (Mørk et al., 1999; Hammer et al., 2019).

Stensiö (1921) first described a bonebed and its fish fauna between the Fish niveau and the Lower Saurian niveau, located to be 33 m above the Fish niveau. The name Grippia niveau was used after Wiman (1929) described the ichthyosaur *Grippia longirostris* from this bonebed. The Grippia niveau Bonebed is a sandstone layer, which has a maximum thickness of 5 cm. The bonebed consists of fossils of marine vertebrates, e.g. Ichthyosaurs, various fish taxa, as well as conodonts (Hansen et al., 2018).

The stratigraphic position of the *Grippia* Bonebed of Marmierfjellet was determined by Hansen et al. (2018) using chemostratigraphic correlation with localities in Ledalen and Sassendalen (Figure 3). These correlations suggested that the bonebed belongs to the ammonoid zone, either the *Bajarunia euomphala* Zone or the *Parasibirites grambergi* Zone, which indicate that the bonebed is of Early- or Early/Middle Spathian age (Figure 2). Findings of un-reworked conodonts in the bonebed support a Spathian age. The thinness of the bed can be a result of either low sedimentation or erosion, reworking and re-sedimentation, both indicative of a sea level rise. Vanadium and Total Organic Carbon (TOC) values indicate that the bonebed was deposited in an increasingly anoxic environment.

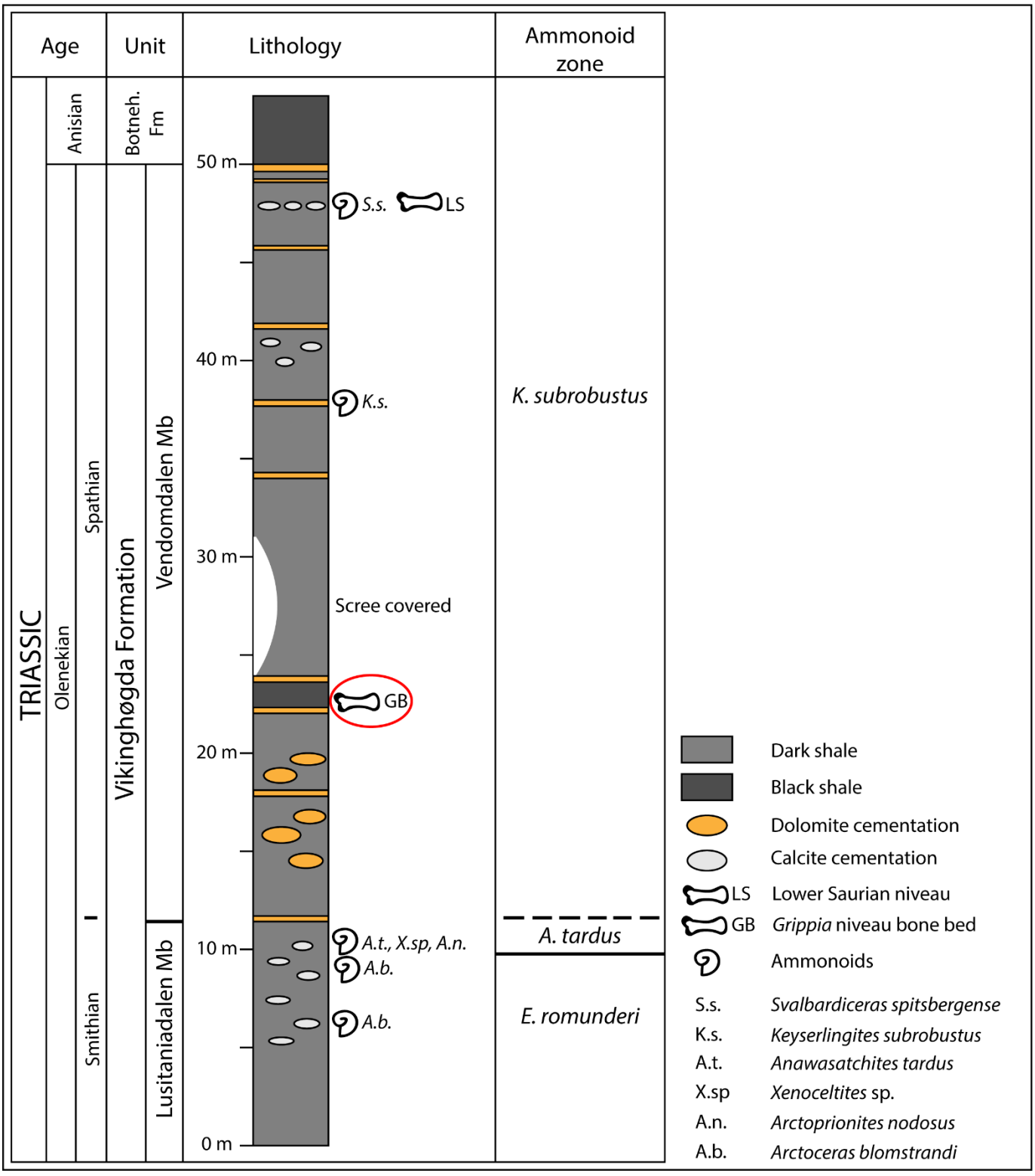

Figure 2 - Stratigraphic log of the Vikinghøgda Formation, of Marmierfjellet, Spitsbergen. The *Grippia* niveau Bonebed is marked with a red circle. Modified from Hansen et al. (2018).

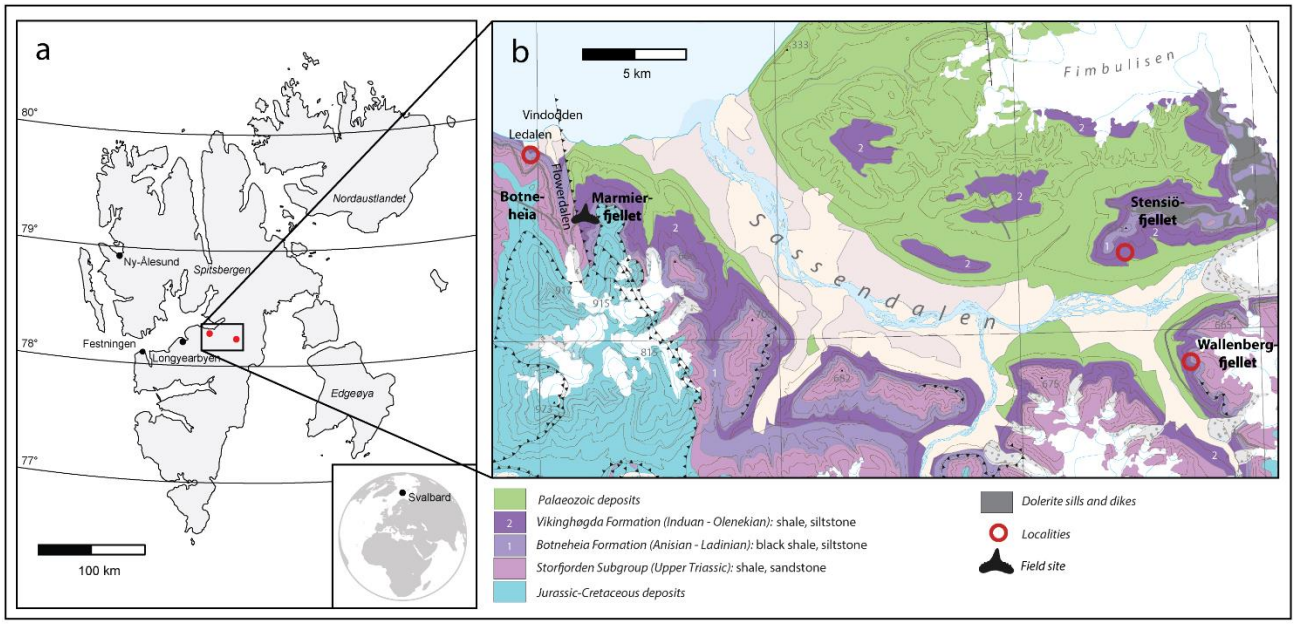

Figure 3 - Map of Svalbard with a detailed stratigraphic map of the field site of 2016 (shark tooth) and localities used for chemostratigraphic correlations (red circles). Modified from Hansen et al. (2018).

2.2 Methods

2.2.1 Sorting

6000 shark teeth were already sorted out from the bonebed and put into boxes based on their size, by volunteers at the Natural History Museum (NHM). For this project further sorting based on morphology was done. The teeth were studied under a magnifying glass. All teeth that were possible Neoselachii were picked out. In the end 360 possible Neoselachii teeth were found. The 360 teeth were chosen based on which teeth were morphologically similar to the ones described as Synechodontiform sp. (1) and Synechodontiform sp. (2) by Bratvold et al. (2018). Broken specimens were glued together with ethyl-2-cyanoacrylate, a liquid with low viscosity that hardens fast.

2.2.2 Picturing

For photographing a Nikon D850 with the Nikon AF-S Micro NIKKOR 60mm f/2.8G ED lens was used. Photos were taken with an automatic shift focus to ensure the whole specimen was in focus. The camera was manually focused on the highest point of the tooth, and depending on the topography of the tooth between 10 to 30 pictures were taken with a focus distance set to

four. The shift focus is dimensionless. For the smallest specimens Nikon D5100 connected to Leica MZ16 A was used. The camera was controlled with DigiCamControl V2.1.1.0 and shift focus had to be done manually to ensure focus on all parts of the tooth.

Photo stacking was done by using Adobe Photoshop CS6 (64 bit) and Helicon Focus 7, preferably Helicon Focus 7 as it is the fastest option. Adobe Illustrator CS6 (64 bit) was used for scaling and making the finished plates.

Thin sections were photographed with the Leica MC170 HD (controlled by DigiCamControl V2.1.1.0) on a Leica DMLP microscope.

The smaller specimens are usually darker in thin sections. Two of them, PMO 235.661 and PMO 235.665 were so dark that with normal picturing no structures could be seen. With High Dynamic Range (HDR) processing the structures came to sight. 10-15 pictures with different light exposures were taken. From over-exposed to under-exposed. Then they were uploaded in Photomatix 6.1, where HDR processing was done. This results in an unnatural look of the picture, but it was necessary to be able to get all the structures in the picture.

2.2.3 Thin section- and Scanning Electron Microscope preparations

To prepare the samples for Scanning Electron Microscope (SEM)-imaging and thin sections they were cast in epoxy. This ensured correct positioning for the surfaces. To make the cast, Struers EpoFix Kit was used. EpoFix Resin was mixed with EpoFix Hardener with a 25:3 mixing ratio in weight and mixed slowly to prevent air bubbles. The teeth were positioned in a plastic container with the help of modelling clay, and then the EpoFix mixture was poured over and left to dry for a minimum of 24 hours at room temperature. When the epoxy cast was dry the plastic containers with the teeth were cut with a wet abrasive saw to isolate each tooth. Then they were polished down to the preferred section using grain size (FEPA P) 120 and 500 on a Struers Knuth Rotor. Before SEM-imaging the sections were etched in 10% HCl for 120 seconds to reveal the crystalline structures in the enameloid and coated with an approximately 20 nm thick carbon layer to prevent charging.

20 samples were sent to the Department of Geosciences at the University of Oslo, where the thin sections were made with a thickness of 45 µm. PMO 235.648-235.656 were first sent to

the thin section lab and studied in SEM afterwards on the remaining material. Unfortunately, due to the small size of the teeth, not all samples had remaining enameloid. Samples without remaining enameloid, except PMO 235.652 and PMO 235.654, are excluded from the study. Because of this PMO 235.659-235.668 were first studied in SEM before making thin sections, to ensure the presence of enameloid.

2.2.4 Computer Tomography

Computed Tomography (CT)-imaging was done with the X-TEK XTH225ST. Three teeth were studied with the CT. For PMO 236.400, 3016 projections were taken, and 2216 projections of PMO 241.385, with four frames pr. projection. 3338 projections, with two frames pr. projection, were taken of PMO 241.470. Multi slice (ms) was set to 1000 (Table 1) and a 0.1 mm aluminium filter was used. The pictures were then uploaded and examined in Avizo, using OrthoSlice and Volume Rendering.

Table 1 - CT-data for PMO 236.400, PMO 241.385 and PMO 241.470.

PMO-number	Projections	Frames pr. projection	Multi slice
236.400	3016	4	1000
241.385	2216	4	1000
241.470	3338	2	1000

2.3 Shark tooth morphology

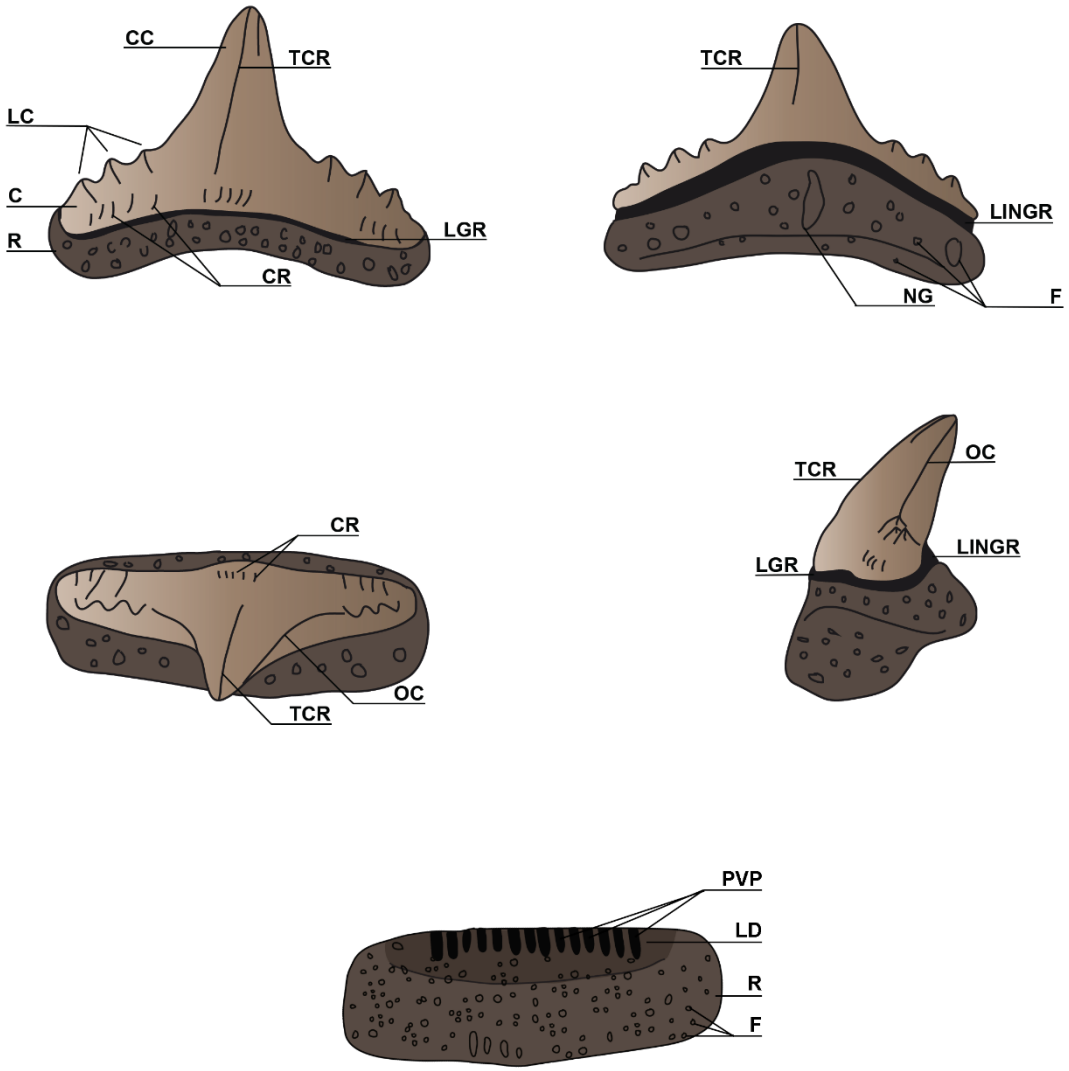

Figure 4 - General drawing of a chondrichthyan tooth (based on PMO 241.300) in labial-, lingual-, occlusal-, mesio-distal- and basal view showing different morphological descriptive terms. Abbreviations: C: Crown, CC: Central cusp, CR: Crest, F: Foramen, LC: Lateral cusplet, LD: Labial depression, LGR: Labial groove, LINGR: Lingual groove, NG: Nutrient groove, OC: Occlusal crest, PVP: Pseudopolyaulacorhize root vascularization pattern, R: Root, TCR: Transverse crest.

This work will describe morphotypes of shark teeth. Because of ontogenetic and sexual dimorphism, identifying species by tooth morphology alone can be misleading (Purdy and Francis, 2007). *Lamna nasus*, an extant mackerel shark (Lamniformes) with similar tooth morphology to the synechodontiform *Synechodus*, shows a wide range of variation in tooth morphology from an embryonic state to adult specimens (Purdy and Francis, 2007). A study by Straube and Pollerspöck (2020) on the dogfish shark (Squaliformes) *Etmopterus spinax* found that males typically develop a higher amount of lateral cusplets and a higher amount of total teeth number, while females usually have teeth larger in size.

The terms used to describe the morphological features of a shark tooth (Figure 4) follow the terminology of Koot (2013) and Bratvold et al. (2018). Descriptions of the teeth will be given in labial-, lingual-, basal- and occlusal view, or along the different axes of the tooth (Figure 5), due to the difficulties of assigning the teeth to a right or left transverse row in the jaw.

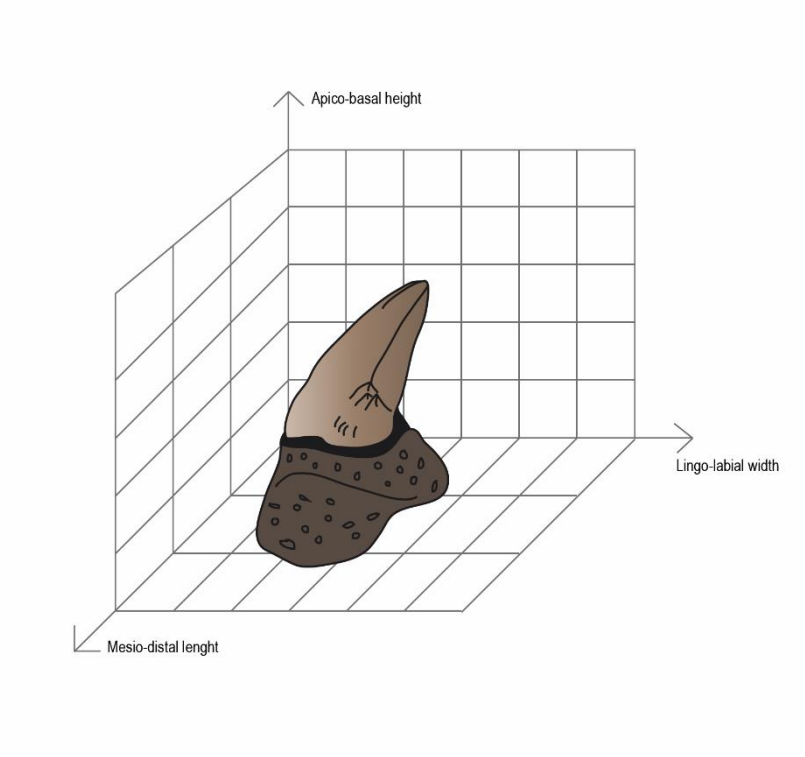

Figure 5 – Axes of a Chondrichthyan tooth; mesio-distal, apico-basal and lingo-labial. Respectively corresponding to length, height and width.

2.4 Dentinal histology and enameloid microstructures of Synechodontiformes

As the chondrichthyan fossil record is dominated by dental material, chondrichthyans are often recognized based on tooth morphology. However, some species have similar morphology and indistinct differences. Therefore, dental histology and enameloid microstructures are good supplements to help identify species.

2.4.1 Dentine

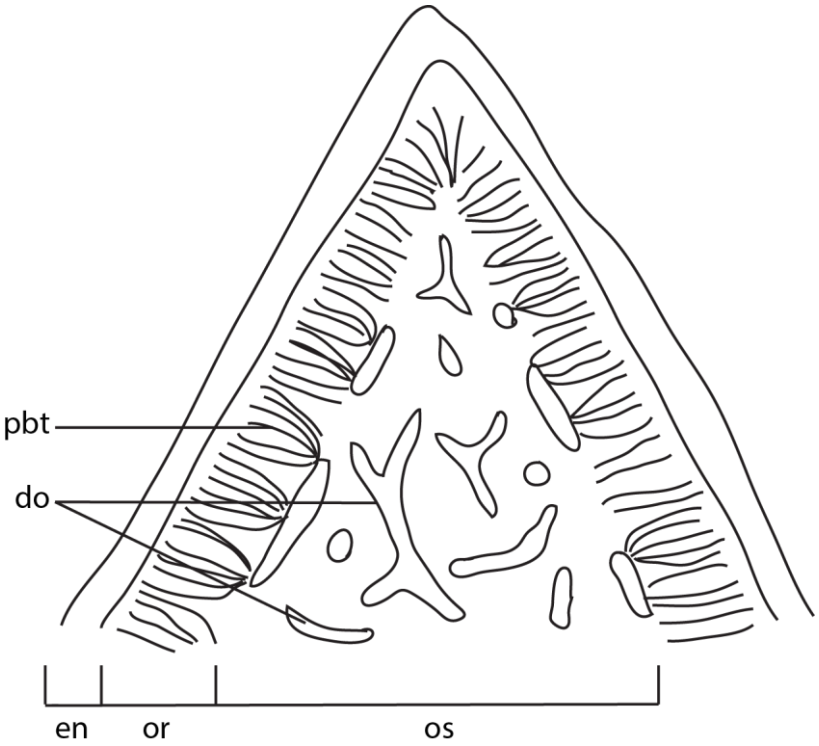

Figure 6 - General drawing of a Chondrichthyan tooth showing the different dental tissues and structures. Redrawn from Radinsky (1961) with updated terminology from Jambura (2020). Abbreviations: do: Denticular osteons, en: Enameloid, or: Orthodentine, os: Osteodentine, pbt: Parallel branching tubules.

The dentinal histological mineralization patterns are divided into three histotypes; orthodont, osteodont and pseudoosteodont. Orthodont histotype means that the dentine consists of only orthodentine (formerly called pallial dentine). Orthodentine is characterized by its parallel branching tubules (Radinsky, 1961; Jambura et al., 2020) (Figure 6). These are linear structures perpendicular to the enameloid. An osteodont histotype consists of only osteodentine, which is recognizable by its denticular osteons (Radinsky, 1961; Smith and Sansom, 2000; Jambura et

al., 2020) (Figure 6). However, if both the orthodentine and osteodentine are present, the histotype is pseudoosteodont (Jambura et al., 2020).

Klug (2010) concluded that Synechodontiformes is a monophyletic group. A recent study on three genera of synechodontiforms by Jambura et al. (2020) shows that they share similar characteristics in tooth histology, all three genera studied are pseudoosteodont. In the centre of the tooth crown is the pulp cavity like in all vertebrate teeth. Covering the pulp cavity is the dentine. The dentine consists of two layers; osteodentine and orthodentine. The osteodentine penetrates the pulp cavity, filling it so that only a narrow hollow central canal remains of the pulp cavity (Jambura et al., 2020). The external layer of the crown, the enameloid, is made up of hypermineralized tissue and capsules the dentine (Jambura et al., 2020).

2.4.2 Enameloid

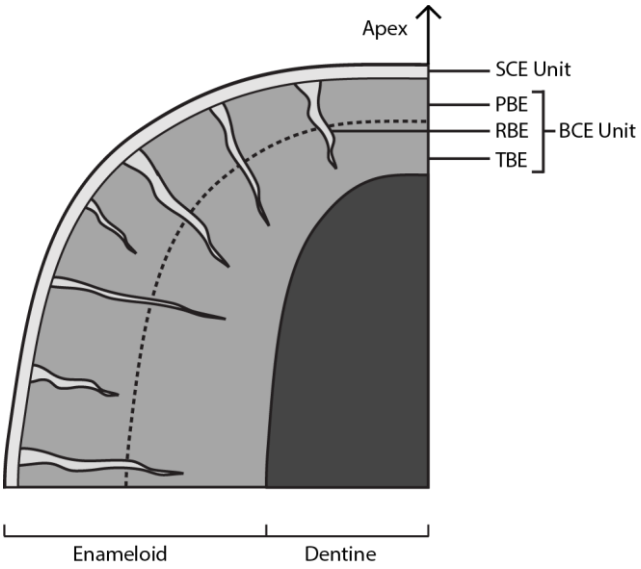

Figure 7 - Generalized drawing of the neoselachian triple-layered enameloid. Abbreviations: BCE: Bundled crystallite enameloid, PBE: Parallel bundled enameloid, RBE: Radial bundled enameloid, SCE: Single crystallite enameloid, TBE: Tangled bundled enameloid. Modified from Enault et al. (2015).

The hard cover of the crown of a shark tooth is enameloid. Enameloid is the ancestral tissue that enamel is derived from (Miake et al., 1991). Lower vertebrates like fish and larval amphibians have enameloid, while higher vertebrates like mammals, reptiles and adult amphibians have enamel (Herold et al., 1989; Miake et al., 1991). The structural differences

between the two tissues are based on which protein the tissue consists of. Enameloid consist mainly of the protein enamelin. The evolution from enameloid to enamel involves the development of the protein amelogenin (Herold et al., 1989).

One synapomorphy for neoselachians, and therefore synechodontiforms, is a triple-layered enameloid (Cuny et al., 2001; Cuny and Risnes, 2005; Guinot and Cappetta, 2011; Enault et al., 2015) (Figure 7). This characteristic gives another criterion apart from morphology alone to distinguish the neoselachians from sister groups, such as Hybodontiformes. The outer layer, the *Single Crystallite Enameloid* (SCE), is a homogenous layer composed of apatite crystallites with random orientation (Cuny et al., 2001; Enault et al., 2015). The inner layers are the *Parallel Bundled Enameloid* (PBE) and the *Tangled Bundled Enameloid* (TBE). Crystallites in these layers connect in bundles. There is no distinct border between these two, so they are regularly referred to as the *Bundled Crystallite Enameloid* (BCE). Inside the BCE some taxa possess radial bundles perpendicular to the SCE and BCE, these bundles make up the *Radial Bundled Enameloid* (RBE) (Enault et al., 2015).

Institutional abbreviations:

PMO – Paleontological Museum Oslo (Natural History Museum, University of Oslo)

Abbreviations used in the description:

BCE – Bundled crystallite enameloid
PBE – Parallel bundled enameloid
SCE – Single crystalline enameloid
TBE – Tangled bundled enameloid

3. Results: Description and comparison of material

All teeth described in the systematic descriptions below belong to the subcohort Neoselachii, the true sharks and rays. Neoselachians have the unique triple-layered enameloid. Batomorphs and some Synechodontiform genera lack the tangled bundled enameloid (TBE), and therefore it is the parallel bundled enameloid (PBE) that is considered the synapomorphy for neoselachians.

Synechodontiformes is an order within neoselachians. Their morphology is characterized by having ornamentation (crests) at the base of the crown, a well-defined central cusp and a flat to concave root base. Characteristics separating them from other neoselachians are the pseudopolyaulacorhize root vascularization pattern: open canals parallel to the lingo-labial axis and it is paired with a labial root depression.

Table 2 - Measurement of the described teeth in this study. *Measured to the point of fracture. na - not available

Species	PMO-number	Mesio-distal [mm]	Apico-basal [mm]	Lingo-labial [mm]
Synechodus sp.	233.882	12.5	6.9	2.5
"	235.656	11.0	6.0	4.0
"	235.662	15.7	6.8*	1.7
"	235.664	19.2	4.0*	2.2
"	235.668	17.0	5.5*	3.1
"	241.300	10.0	6.5	2.8
"	241.301	5.9	4.0	1.5
"	241.302	7.2	5.8	2.1
"	241.303	8.3*	6.0	2.5
Synechodus incrementum	235.652	5.0*	4.0	2.0
"	235.661	4.0*	1.8	1.5
"	235.665	11.5	2.5	1.1
Rhomphaiodon minor	235.667	7.0*	5.0	3.9
"	236.400	11.0*	8.0*	4.0
"	241.304	14.5	10.5	5.8
"	241.386	10.1*	6.5	3.8
"	241.387	10.0	6.0*	4.2
"	241.388	10.1	4.2	3.3
Rhomphaiodon nicolensis	235.663	10.5	6.5*	4.0
"	243.000	16.4	9.0	5.5
"	243.001	9.1	6.0*	na
Grozonodon sp.	235.654	6.0*	6.0	3.0
"	235.659	8.7*	10.4*	1.7
"	241.385	8.2*	6.0	3.4
"	241.470	13.6	5.5	4.7

Table 3 - Schematic description of different morphological traits on the crown. See Figure 4. Lateral cusplets are divided due to different numbers on each side of the central cusp. The first listed number is the left side seen from labial view. na – Not available. Abbreviations: CC, Central cusp; CR, Crest; LC, Lateral cusplet; LF, Labial face; LGR, Labial groove; LIF, Lingual face; LINGR, Lingual groove; OC, Occlusal crest; TCR, Transverse crest.

Species	PMO-number	LC	OC	LGR	LINGR	LF	LIF
Synechodus sp.	233.882	3 | 0	sharp	deep	shallow	CR	CR
"	235.656	na | 3	sharp	deep	shallow	CR	CR
"	235.662	2 | 5	sharp	deep	shallow	CR	CR
"	235.664	7 | 6	sharp	deep	shallow	CR	CR
"	235.668	4 | 6	sharp	deep	shallow	smooth	CR
"	241.300	4 | 3	sharp	deep	shallow	smooth	smooth
"	241.301	2 | 1	sharp	deep	shallow	smooth	smooth
"	241.302	1 | 1	sharp	deep	shallow	weak TCR	weak TCR
"	241.303	na | 5	sharp	deep	shallow	CR and weak TCR	CR and weak TCR
Synechodus incrementum	235.652	na | na	sharp	deep	shallow	Weak TCR on CC and all LC	Weak TCR on CC and all LC
"	235.661	na | 3	sharp	shallow	deep	TCR on CC and all LC	TCR on CC and all LC
"	235.665	9 | 6	sharp	shallow	deep	TCR on CC and all LC	TCR on CC and all LC
Rhomphaiodon minor	235.667	na | 2	sharp	deep	shallow	CR	CR
"	236.400	1 | 1	sharp	deep	shallow	CR	CR
"	24.304	1 | 4	sharp	deep	shallow	CR	CR
"	241.386	na | 5	sharp	deep	shallow	CR and weak TCR	CR and weak TCR
"	241.387	2 | 0	sharp	deep	shallow	CR	CR
"	241.388	3 | 3	sharp	deep	shallow	CR and TCR	TCR
Rhomphaiodon nicolensis	235.663	na | 5	sharp	shallow	na	CR	na
"	243.000	3 | 3	sharp	shallow	shallow	CR and TCR	CR and TCR
"	243.001	3 | 2	na	shallow	na	CR	na
Grozonodon sp.	235.654	na | na	sharp	deep	shallow	CR	CR and TCR
"	235.659	na | na	serrated	deep	shallow	CR	CR and TCR
"	241.385	0 | na	serrated	deep	shallow	CR	CR and TCR
"	241.470	0 | 0	serrated	na	deep	TCR	CR and TCR

3.1 *Synechodus* sp.

Class	**Chondrichthyes** Huxley 1880
Subclass	**Elasmobranchii** Bonaparte 1838
Cohort	**Euselachii** Hay 1902
Subcohort	**Neoselachii** Compagno 1997
Order	**Synechodontiformes** Duffin and Ward 1993
Family	**Paleospinacidae** Regan 1906
Genus	**Synechodus** Woodward 1888

Synechodus sp.

Identified on the basis of the following synapomorphies and apomorphies:

1. Triple-layered enameloid, including radial bundles
2. Pseudopolyaulacorhize root vascularization pattern
3. Labial root depression
4. Similar crown morphology to other *Synechodus* species

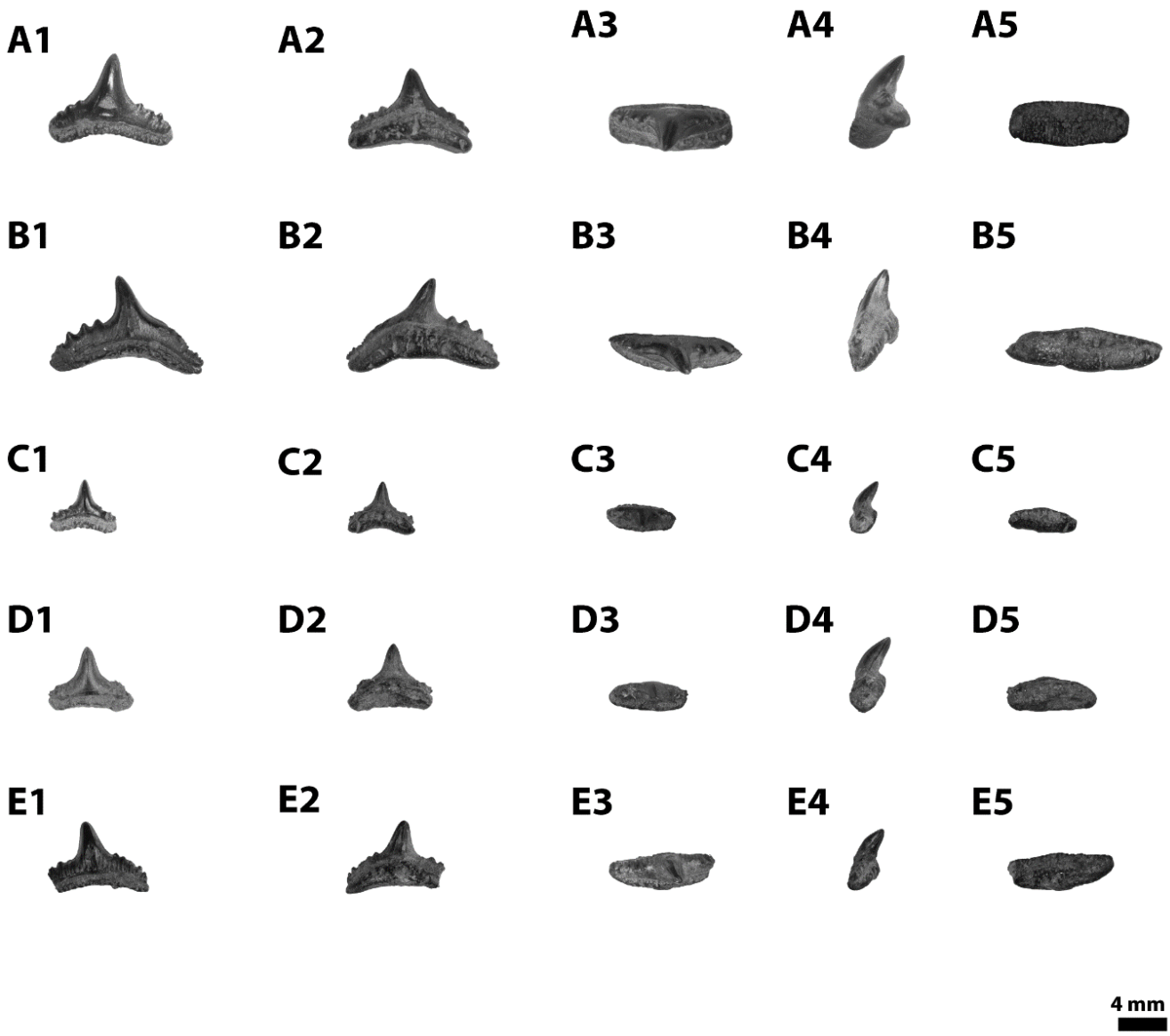

Figure 8 – *Synechodus* sp.

A, PMO 241.300; B, PMO 233.882; C, PMO 241.301; D, PMO 241.302; E, PMO 241.303. 1, Labial view; 2, Lingual view; 3, Occlusal view; 4, Mesio-distal view; 5, Basal view

Material:

20 isolated teeth, seven of them are complete and 13 are broken to various degree. PMO 233.882, PMO 235.662, PMO 235.656, PMO 241.300, PMO 241.301, PMO 241.302, PMO 241.303, PMO 235.664, PMO 235.668 (Figure 8 and 9)

Description:

The mesio-distal length is between 5.9-19.2 mm (Table 2). The apico-basal height, measured

from the base of the root to the apex of the central cusp, is between 4.0-6.9 mm. The base of the crown forms a convex arch and is highest under the central cusp. The central cusp has a sharp apex and is lingually inclined in all samples. In PMO 233.882 (Figure 8-B) and PMO 241.303 (Figure 8-C), the central cusp is also mesially tilted. Between one and seven lateral cusplets are found on all specimens (Table 3), and they are typically considerably lower than the central cusp. The exception is PMO 235.664 (Figure 9-C1) and PMO 235.668 (Figure 9-D1), which are flattened in the apico-basal axis. Some of the cusplets appear more as an elevation of the crown, for example in PMO 235.662 (Figure 9-A1). The smallest teeth have a completely smooth crown surface, but the bigger ones possess small crests radiating vertically from the base of the crown. A sharp occlusal crest forms a cutting edge of the crown. The root, compared to the crown, is generally thin and has a concave arch that follows the crown. The labial groove is deep, while the lingual groove is shallow. The root has a labial depression. Pseudopolyaulacorhize root vascularization patterns are present to various degree. PMO 241.300 (Figure 8-A) and PMO 241.303 (Figure 8-E) are the specimens with the most developed root vascularization pattern. The morphology is similar to the Cretaceous *S. tenuis* described first by Woodward (1889), and a more recent description by Batchelor and Duffin (2020). They are similar by the root vascularization pattern, the smooth surface, pointy and symmetrical central cusp, as well as the concave arch of the lower face of the crown. They differ by the cutting edge; *S. tenuis* has a weak cutting edge in the occlusal crest, while *Synechodus* sp. has a sharp cutting edge. The high number of lateral cusplets and the presumably lower central cusp of PMO 235.664 and PMO 235.668 indicates a more distal placement in the jaw compared to the other teeth. PMO 235.664 and PMO 235.668 differ from *S. incrementum* (Johns et al., 1997) by their smooth crown surface.

Both orthodentine and osteodentine are present in PMO 235.656, PMO 235.662, PMO 235.664 and PMO 235.668. The orthodentine varies in thickness through the mesio-distal length, being thickest at the apex. There is a sharp boundary between the orthodentine and the osteodentine. This indicates a pseudoosteodont histotype (Figure 9). PMO 235.662, PMO 235.664 and PMO 235.668 show growth layers in the orthodentine, respectively, four (Figure 9-A2), three (Figure 9-C2) and four (Figure 9-D2) layers.

SEM-imaging shows a clear SCE and BCE unit. The SCE is usually restricted to the apex or the crests in the enameloid. In PMO 235.662 (Figure 9-A3), both the PBE and TBE are easy to separate. While in PMO 235.656 (Figure 9-B3), PMO 235.664 (Figure 9-C3) and PMO 235.668

(Figure 9-D3) the transition within the BCE unit is indistinct. Radial bundles are present in PMO 235.662, PMO 235.664 and PMO 235.688; they radiate perpendicularly from the SCE and penetrate both the PBE and the TBE. The presence of a well-developed TBE and radial bundles infer a derived enameloid.

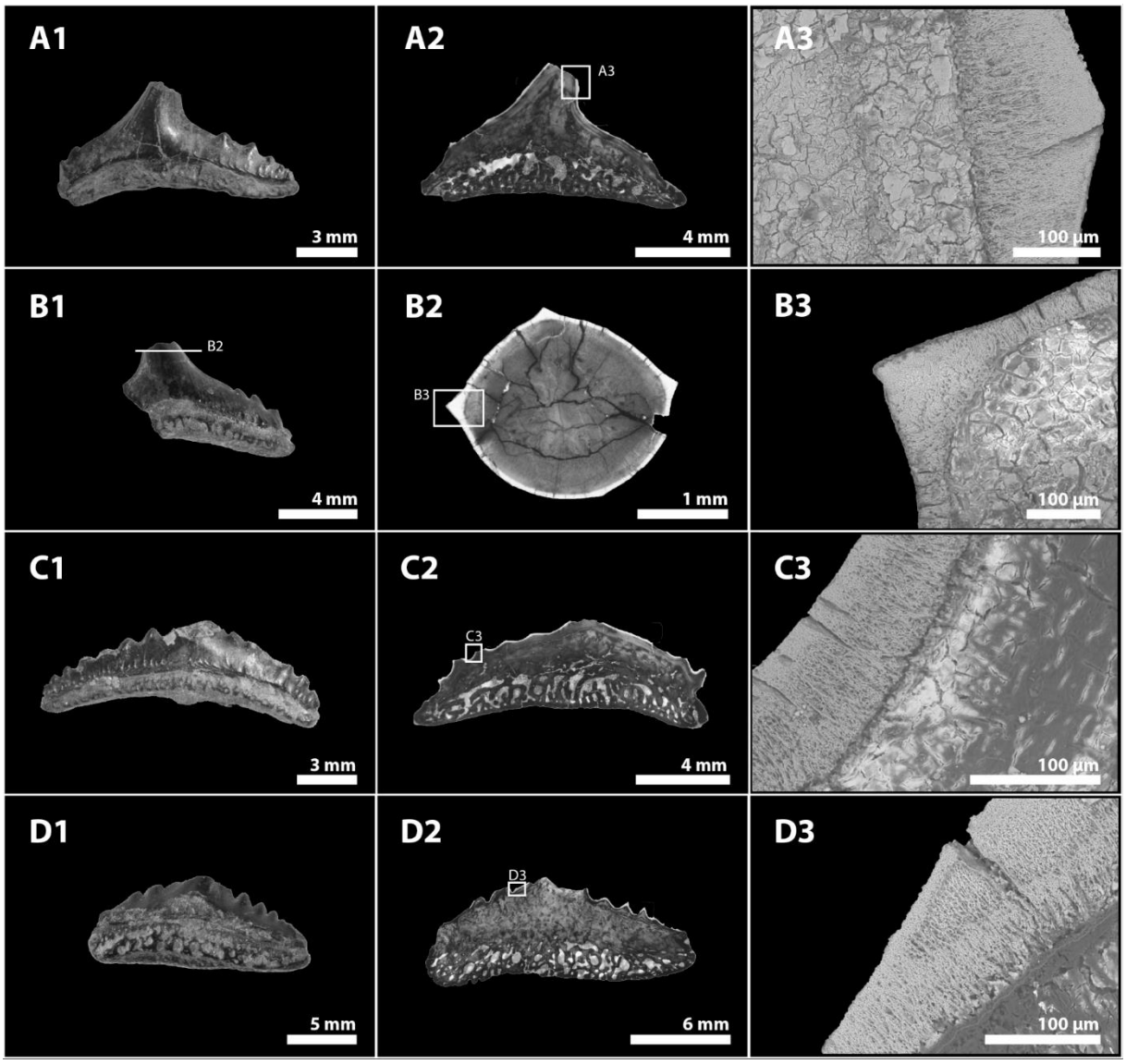

Figure 9 - *Synechodus* sp.

A, PMO 235.662; B, PMO 235.656; C, PMO 235.664; D, PMO 235.668. 1, Tooth in labial view; 2, Thin section showing the dentinal histology; 3, SEM-image of enameloid microstructures. The SCE presents as the outer layer without any arranged structure. PBE is recognized by the parallel orientation of the bundles and the TBE by the haphazardly orientation of the bundles. The radial bundles are present in A3, C3 and D3 and are the bundles that radiate from the SCE and through the BCE.

3.2 *Synechodus incrementum*

Class	**Chondrichthyes** Huxley 1880
Subclass	**Elasmobranchii** Bonaparte 1838
Cohort	**Euselachii** Hay 1902
Subcohort	**Neoselachii** Compagno 1997
Order	**Synechodontiformes** Duffin and Ward 1993
Family	**Paleospinacidae** Regan 1906
Genus	**Synechodus** Woodward 1888

Synechodus incrementum Johns et. al. 1997

Identified on the basis of the following synapomorphies and apomorphies:

1. Triple-layered enameloid
2. Pseudopolyaulacorhize root vascularization pattern
3. Labial root depression
4. Transverse crests reaching the apex of the central cusp and cusplets

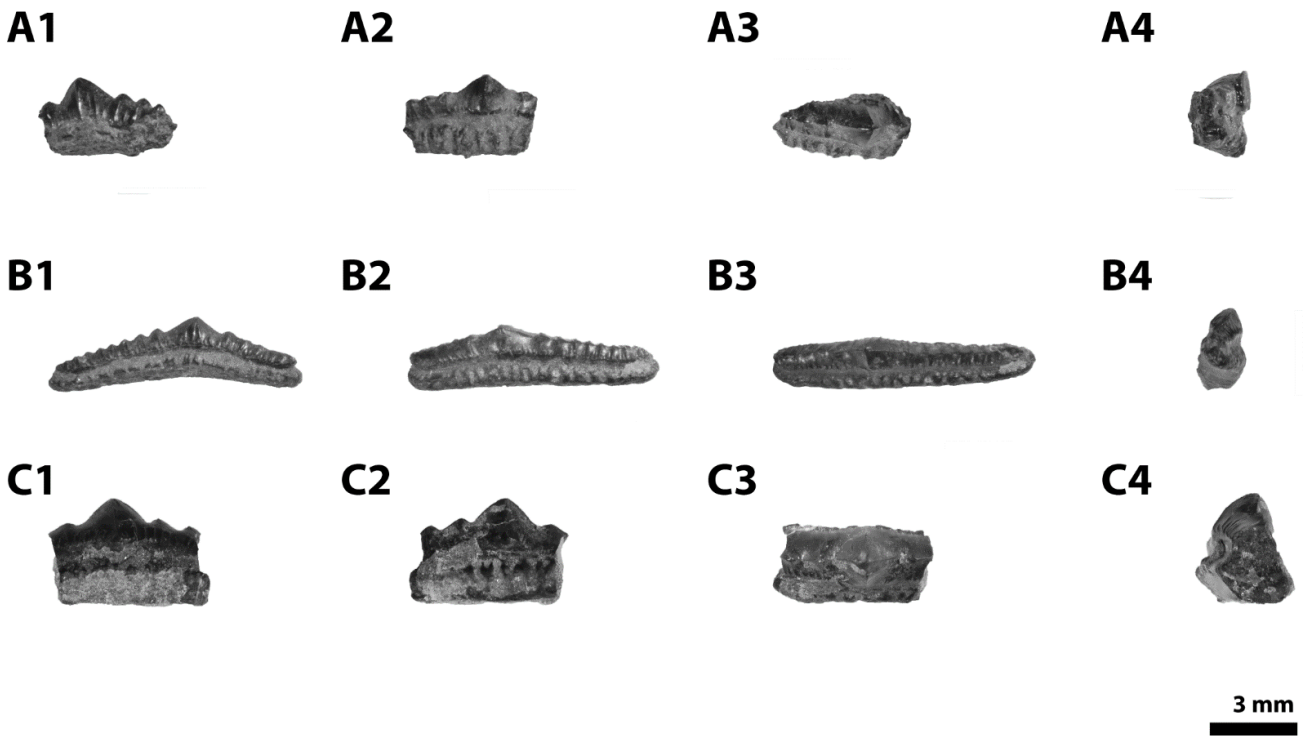

Figure 10 – *Synechodus incrementum*

A, PMO 235.661; B, PMO 235.665; C, 235.652. 1, Labial view; 2, Lingual view; 3, Occlusal view; 4, Mesio-distal view

Material:

Four isolated teeth, one of them is whole. PMO 235.652, PMO 235.661 and PMO 235.665 (Figure 10).

Description:

Only PMO 235.665 is preserved in its full length of 11.5 mm (Table 2). Even though the other teeth are fractured in the mesio-distal axis, they appear to be smaller. In its whole length the crown has many small lateral cusplets, nine at most (Table 3). The central cusp is generally wider and higher than the lateral cusplets (Figure 10). Also, it is not particularly sharp compared to *Synechodus* sp.. The angle at the apex is around 90 degrees. A prominent transverse crest is present on all cusplets, including the central cusp. The transverse crest reaches all the way from the base of the crown to the apex of the cusplets, and is present on both the labial- and the lingual surface. The occlusal crest is present in the whole length of the tooth. The labial groove is shallow and the lingual groove is deep, except for on PMO 235.652 (Table 3). PMO 235.665

is the only specimen with a good enough preserved root to observe the pseudopolyaulachorize root vascularization pattern. The morphology is similar to *S. incrementum* Type D and E described from the Upper Triassic of British Columbia (Johns et al., 1997) by the transverse crests, the size ratio between central cups and lateral cusplets and the root vascularization pattern. The number of lateral cusplets and the reduced height of the central cusp indicate a distal position in the jaw.

Thin sections of both PMO 235.661 (Figure 11-A2) and PMO 235.665 (Figure 11-B2) show very dark dentinal tissue. Both teeth are pseudoosteodont, however, the osteodentine of PMO 235.665 is not very well developed. Only one small dentinal osteon is observed. It has a more dominant orthodentine compared to other studied specimens.

PMO 235.661 (Figure 11-A3) and PMO 235.665 (Figure 11-B3) possess SCE, PBE and TBE. The SCE and PBE have a gradual transition, and it is not a defined boundary. The TBE is thickest at the apex. The remaining SCE is limited to the apex. In PMO 235.665, the dentine partially penetrates the TBE at the apex of the tooth. This penetration from the dentine to the TBE is only seen in one other of the studied samples (*Rhomphaiodon minor*, PMO 235.667).

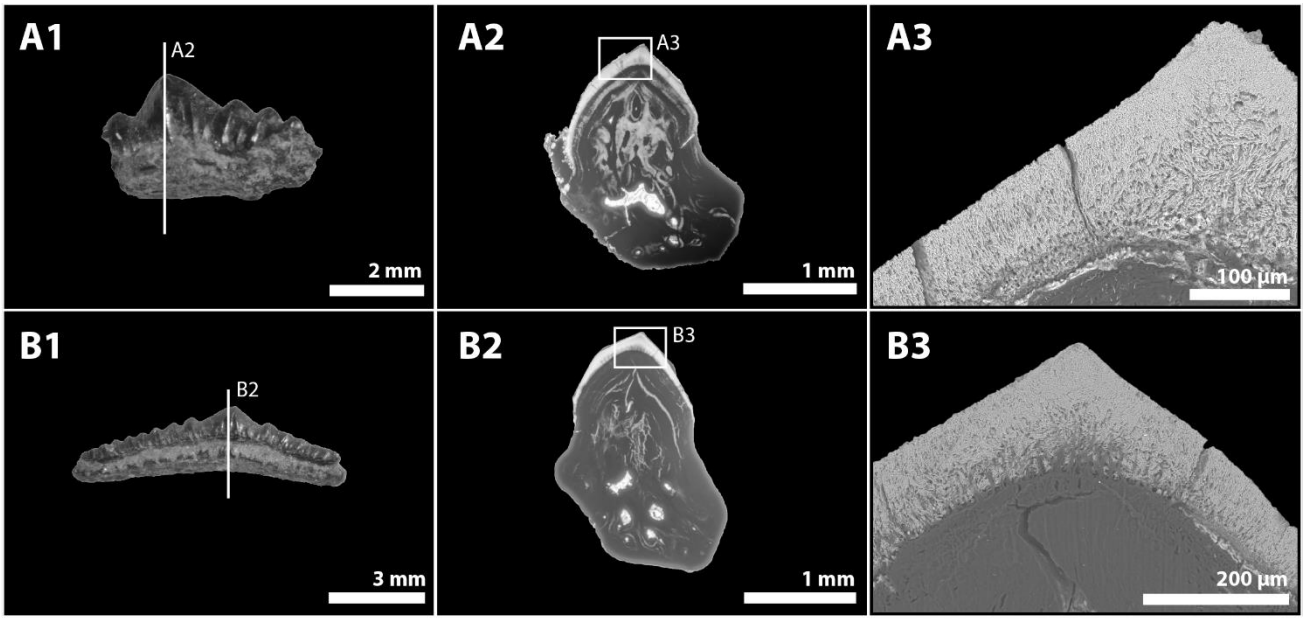

Figure 11 - *Synechodus incrementum.*

A, PMO 235.661 and B, PMO 235.665. 1, Tooth in labial view; 2, Thin section showing the dentinal histology (photos are HDR processed); 3, SEM-image of the enameloid microstructures. SCE is present at the apex. PBE is the layer beneath the SCE, and the TBE is most prevalent at the apex.

3.3 *Rhomphaiodon minor*

Class	**Chondrichthyes** Huxley 1880
Subclass	**Elasmobranchii** Bonaparte 1838
Cohort	**Euselachii** Hay 1902
Subcohort	**Neoselachii** Compagno 1997
Order	**Synechodontiformes** Duffin and Ward 1993
Family	*Incertae sedis*
Genus	**Rhomphaiodon** Duffin 1993

Rhomphaiodon minor Duffin 1993

Identified on the basis of the following synapomorphies and apomorphies:

1. Triple-layered enameloid with indistinct differences in the BCE Unit.
2. Pseudopolyaulacorhize root vascularization pattern
3. Labial root depression
4. Rounded apices of central cusp and cusplets
5. Heavily ornamented crown

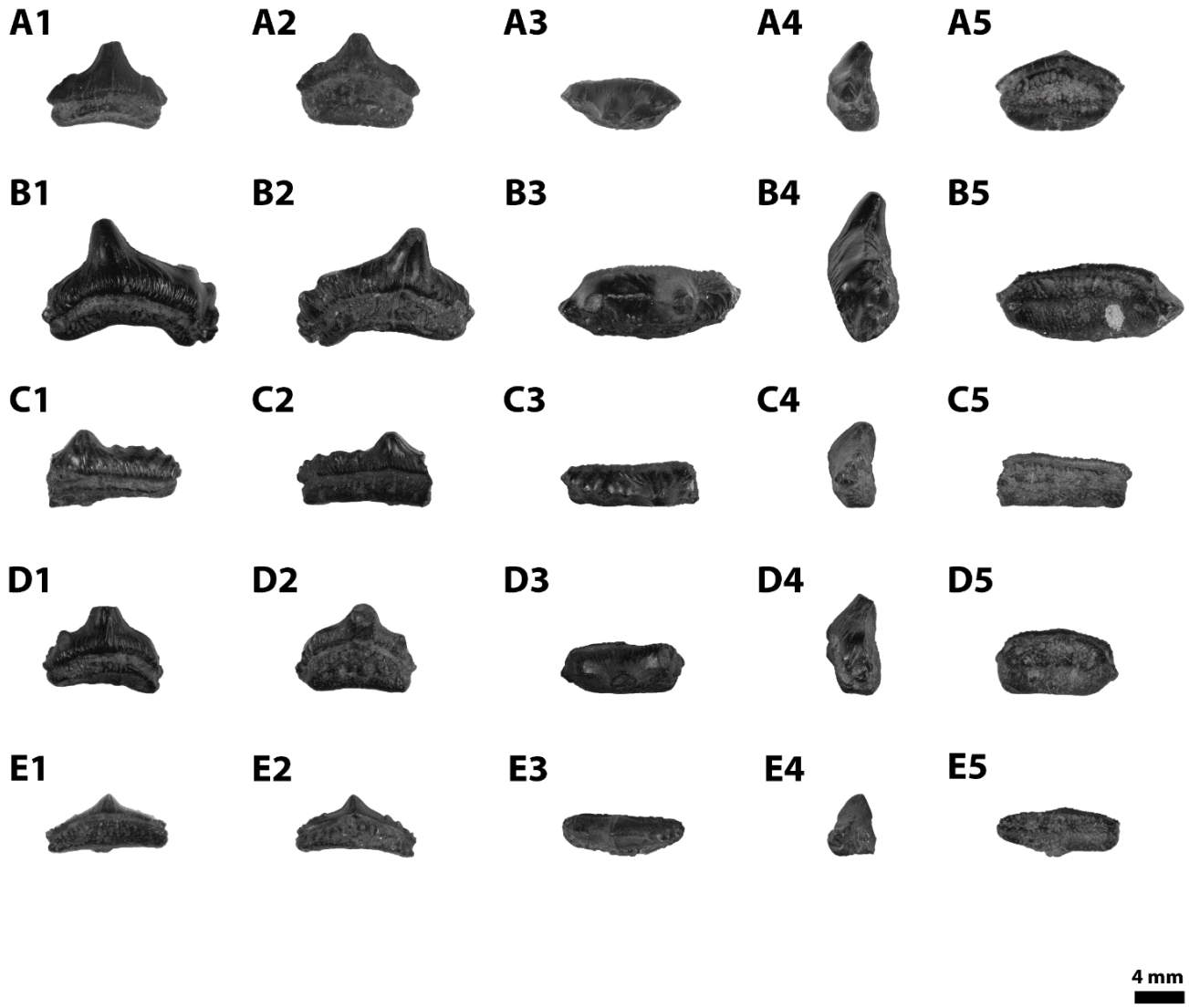

Figure 12 – *Rhomphaiodon minor*

A, PMO 236.400; B, PMO 241.304; C, PMO 241.386; D, PMO 241.387; E, PMO 241.388. 1, Labial view; 2, Lingual view; 3, Occlusal view; 4, Mesio-distal view; 5, Basal view

Material:

27 isolated teeth, one covered by matrix. PMO 235.667, PMO 236.400, PMO 241.304, PMO 241.386, PMO 241.387 and PMO 241.388 (Figure 12)

Description:

The length of the teeth varies from 7.0-14.5 mm (Table 2); however, there are some poorly preserved specimens that appear both larger and smaller than this. The crown consists of a prominent central cusp, and none to four lateral cusplets that usually are situated on the very ends of the mesio-distal axis. The number of lateral cusplets is not the same on each side of the central cusp (Table 3). In general, the crown is lingually angled. The labial face of the crown is distinctly convex, and the apices of the central cusp and lateral cusplets are rounded. Small crests are radiating apically from the base of the crown, and a weak transverse crest is present in some specimens. The labial groove is deeply concave. On the lingual face of the crown, the apically radiating crests from the basal of the crown are coarser compared to the labial side. The lingual groove is not as deep as the labial groove, and the root makes up half of the apico-basal height on the lingual side as opposed to on the labial side where it appears as a thin layer beneath the crown. The root has many small foramina. From a basal view, the labial root depression, with pseudopolyaulacorhize root vascularization pattern parallel to the lingo-labial axis, is observed. This root morphology is identical to the ones described by Klug (2010), of *Rhomphaiodon minor*. PMO 241.386 (Figure 12-C) has similar crown morphology and ornamentation to *Synechodus rhaeticus* described by Cuny et al. (2000), but differs from the one pictured in Cuny and Risnes (2005). The crown ornamentation, rounding of the cusp and cusplets together with the root vascularization is the same as the other *R. minor* teeth described here. The only difference is the apico-basal flattening, which can be explained by heterodonty differences and represent a more distal placement in the jaw.

Histology studies of PMO 235.667 (Figure 13-A2) and 236.400 (Appendix 1) show a pseudoosteodont histotype. The orthodentine is very thin, and most of the dentine consists of osteodentine. Parallel branching tubules are observed in the orthodentine, and many small dentinal osteons in the osteodentine. CT-imaging of PMO 236.400 gives a three dimensional view of the dentine and the interaction between the different dentinal tissues, root and enameloid. The orthodentine appears as a thin layer directly underneath the enameloid that thickens towards the apex of the crown. While osteodentine makes up most of the crown, and the whole root.

SEM-imaging of PMO 235.667 clearly shows SCE, PBE and TBE with indistinct boundaries between the three different layers (Figure 13-A3). The dentine partially penetrates the TBE at the apex of a lateral cusplet.

The morphological and the enameloid microstructures are similar to the *R. minor* described by (Cuny et al., 2000) and Cuny and Risnes (2005). Particularly, the characteristic rounded cusp and cusplet together with the strong ornamentation and the indistinct layering within the BCE unit. However, these are significantly larger.

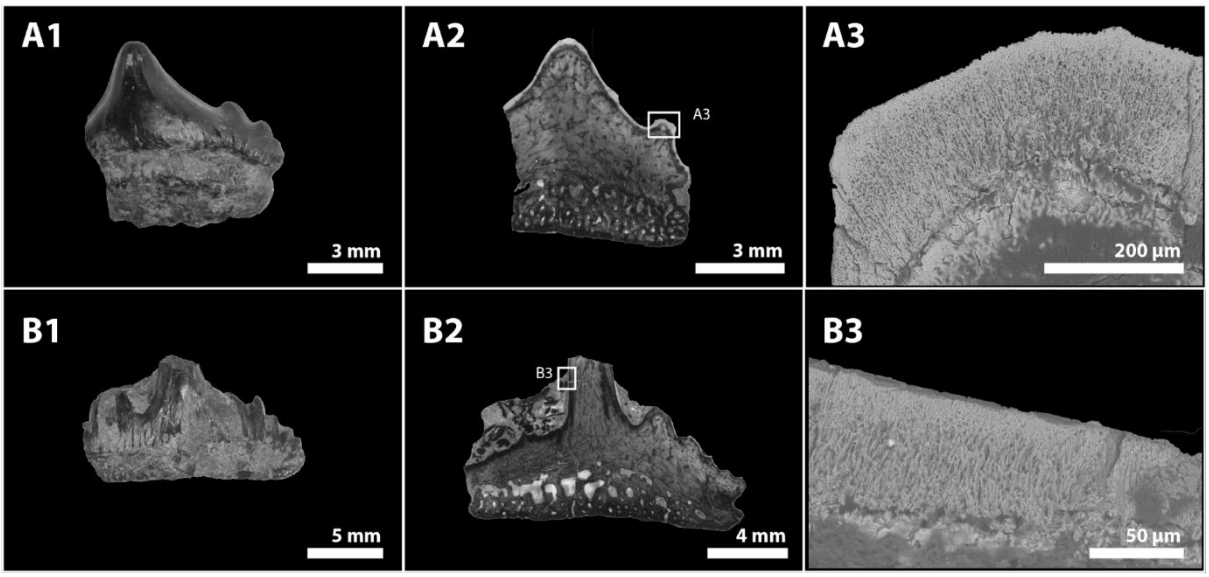

Figure 13 – *Rhomphaiodon minor* (A) and *Rhomphaiodon nicolensis* (B).

A, PMO 235.667 and B, PMO 235.663. 1, Tooth in labial view; 2, Thin section; 3, SEM-image showing the triple-layered enameloid. SCE as the outer layer with respectively PBE and TBE underneath.

3.4 *Rhomphaiodon nicolensis*

Class	**Chondrichthyes** Huxley 1880
Subclass	**Elasmobranchii** Bonaparte 1838
Cohort	**Euselachii** Hay 1902
Subcohort	**Neoselachii** Compagno 1997
Order	**Synechodontiformes** Duffin and Ward 1993
Family	*Incertae sedis*
Genus	**Rhomphaiodon** Duffin 1993

Rhomphaiodon nicolensis Duffin 1993

Identified on the basis of the following synapomorphies and apomorphies:

1. Triple-layered enameloid
2. Pseudopolyaulacorhize root vascularization pattern
3. Labial root depression

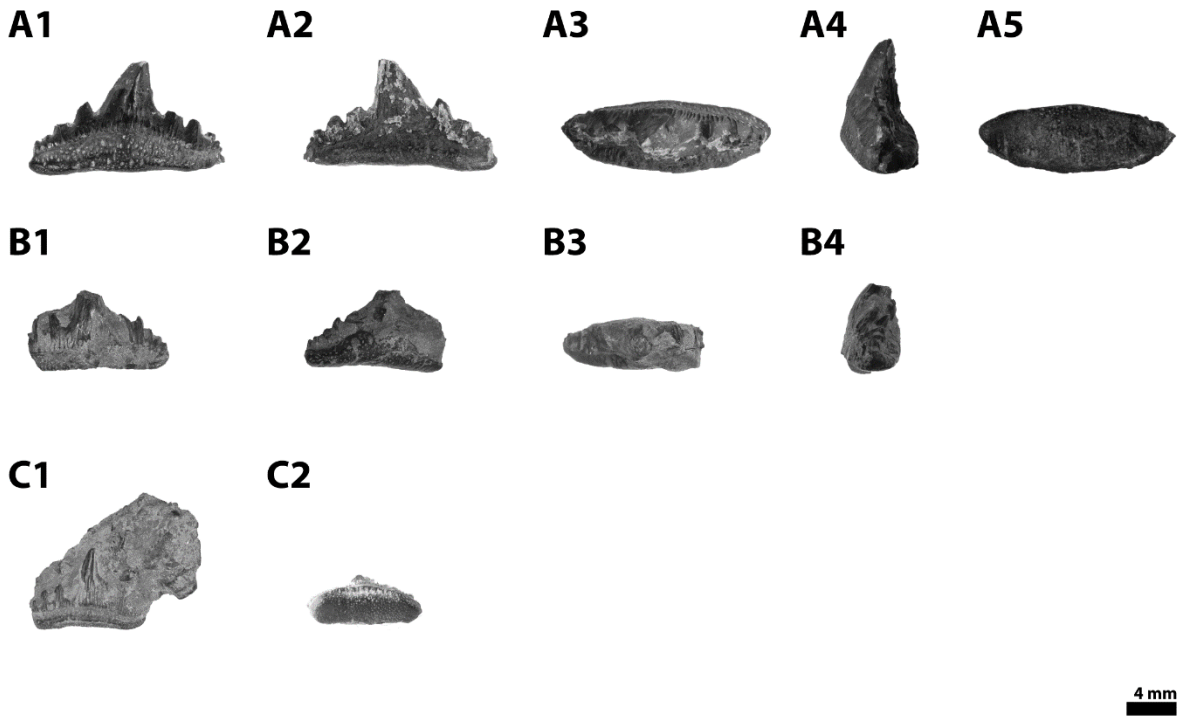

Figure 14 – *Rhomphaiodon nicolensis*

A, PMO 243.000; A1, Labial view; A2, Lingual view; A3, Occlusal view; A4, Mesio-distal view; A5, Basal view; B, PMO 235.663; B1, Labial view; B2, Lingual view; B3, Occlusal view; B4, Mesio-distal view; C, PMO 243.001; C1, Labial view; C2, Basal view.

Material:

One isolated tooth, two covered by matrix. PMO 243.000, PMO 235.663, PMO 243.001 (Figure 14).

Description:

The mesio-distal length of the teeth varies from 9.1-16.4 mm (Table 2). The central cusp is positioned in the centre of the mesio-distal axis. The number of lateral cusplets is between one and five (Table 3), and the lateral cusplets are significantly lower in height compared to the central cusp. Both the apices of the central cusp and the lateral cusplets are sharp and pointy, and in one specimen (PMO 243.000) mesio-distally angled. Compared to *Synechodus* sp. the lateral cusplets present more separated from each other. The labial face of the crown has small vertical crests radiating from the base of the crown and they go no longer up than $\frac{1}{3}$ of the central cusp. A transverse crest is present on the central cusp of PMO 243.000 (Figure 14-A1) and on all of the lateral cusplets of the other studied samples. The lingual face of the crown shows the same ornamentation as on the labial side, except that the crests are reaching further up towards

the apex. Both the labial- and the lingual grooves are shallow, and they appear as thin lines. The labial root depression with pseudopolyaulacorhize vascularization pattern is present in both PMO 243.000 (Figure 14-A5) and PMO 243.001 (Figure 14-C2), being more developed in the latter.

Under the enameloid lies a thin layer of dentine with parallel branching tubules, the orthodentine. The thickness of the orthodentine varies, being the thickest at the apex of the central cusp and the lateral cusplets. The presence of parallel branching tubules also varies. However, there seems to be no pattern in where the tubules are more prominent. Making up most of the crown is the osteodentine, recognizable from its denticular osteons. With both dentinal tissues present, the tooth is pseudoosteodont (Figure 13-B2).

PMO 235.663 has the neoselachian triple-layered enameloid. There is a sharp border between the SCE unit and the BCE unit. The SCE layer is thin. Within the BCE unit, the PBE is the most dominant, while the TBE presents as a thin layer at the base of the enameloid (Figure 13-B3). These enameloid structures are similar to those of *Rhomphaiodon nicolensis* described by Cuny and Risnes (2005).

3.5 *Grozonodon* sp.

Class	**Chondrichthyes** Huxley 1880
Subclass	**Elasmobranchii** Bonaparte 1838
Cohort	**Euselachii** Hay 1902
Subcohort	**Neoselachii** Compagno 1997
Order	*incertae sedis*
Family	*incertae sedis*
Genus	**Grozonodon** Cuny, Martin, Rauscher & Mazin, 1998

Grozonodon sp.

Identified on the basis of the following synapomorphies and apomorphies:

1. Triple-layered enameloid
2. Serrated cutting edge
3. Anaulacorhize root vascularization pattern
4. No lateral cusplets
5. Strong lingual transverse crest

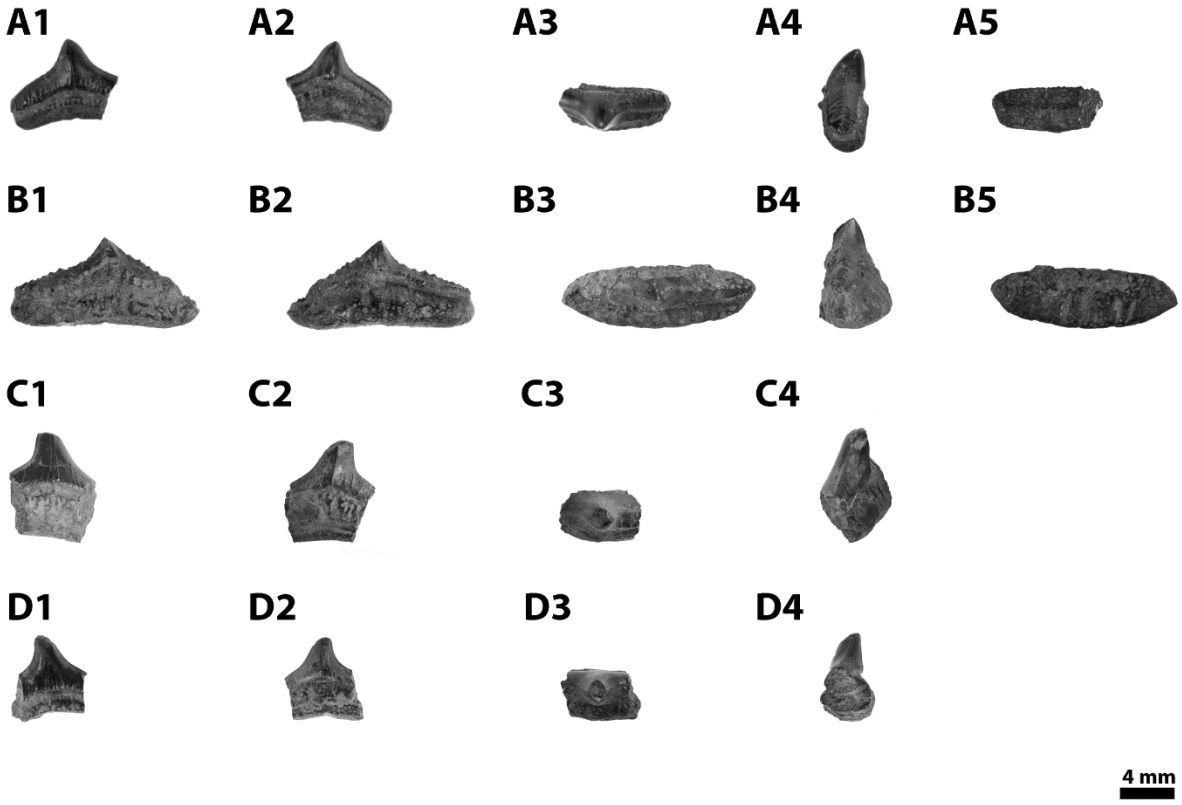

Figure 15 – *Grozonodon* sp.

A, PMO 241.385; B, PMO 241.470; C, PMO 235.659; D, PMO 235.654. 1, Labial view; 2, Lingual view; 3, Occlusal view; 4, Mesio-distal view; 5, Basal view

Material:

Four teeth, broken to various degree. PMO 235.654, PMO 235.659, PMO 241.385, PMO 241.470 (Figure 15).

Description:

The teeth vary from 8.7-13.6 mm in length, and 5.5-10.4 mm in height (Table 2). The central cusp is slightly angled in the lingual and mesio-distal direction. There are no lateral cusplets (Table 3). The occlusal crest forms a sharp cutting edge, and serrations are present. The serrations on PMO 235.659 (Figure 15-C) and PMO 241.385 (Figure 15-A) are small (≤ 200 µm) while on PMO 241.470 (Figure 15-B) they are at most ~ 600 µm. All three teeth have secondary serrations, meaning they consist exclusively of enameloid (Appendix 2). However, PMO 241.470 also exhibit primary serrations, recognized based on the influence of dentine (Appendix 3). PMO 241.385 and PMO 241.471 have a deep gullet serration, while PMO

235.659 have a shallow gullet serration. The occlusal crest on the mesial- or distal end of the crown is more serrated than on the cusp. However, on PMO 241.470 the serrations reach further up towards the apex (Figure 16). The labial face of the crown has small crests radiating apically from the base of the crown in its whole length. A transverse crest on the labial face of the crown is present in various degree on all four samples. PMO 241.470 being the one with the strongest transverse crest and PMO 235.654 has the weakest transverse crest on the labial face, but the lingual transverse crest is sharp. On the lingual face of the crown, a sharp transverse crest is present, as well as some smaller crests radiating apically from the base of the crown. The labial groove is deep and the lingual groove is shallow. The root has a labial depression. It has rather randomly located foramina, representing an anaulacorhize vascularization pattern, (Figure 15-A5). PMO 241.470 has additionally deep grooves perpendicular to the mesio-distal axis, on the lingual side of the root. The minimal crown ornamentation, anaulacorhizy root with a labial depression and the loss of lateral cusplets are similar to the genus *Grozonodon* as described by Cuny et al. (1998), and from the Norian of France and by Sander et al. (2016) from the Rhaetian of Germany. The sharp transverse crest, absence of radial bundles and the serrated cutting edge differ, indicating a different species within the genus *Grozonodon*.

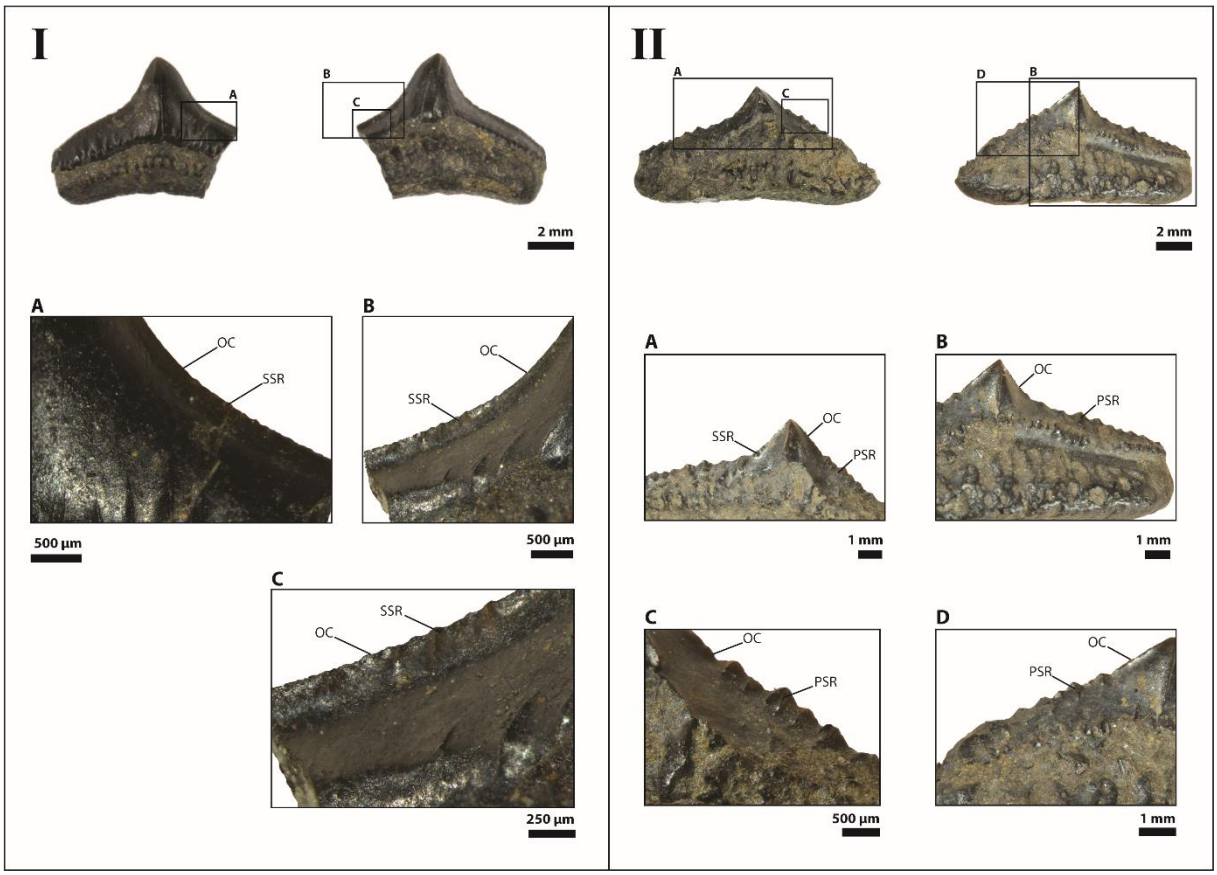

Figure 16 – *Grozonodon* sp. I, PMO 241.385; II, PMO 241.470. The serrated cutting edge of *Grozonodon* sp. seen from both labial- and lingual view. Abbreviations: OC, Occlusal crest; PSR, Primary serration; SSR, Secondary serration.

Grozonodon sp. is pseudoosteodont, possessing both orthodentine and osteodentine. The orthodentine layer is relatively thick and contains parallel branching tubules. The osteodentine lies underneath. There is a clear border between the two dentinal tissues (Figure 17-2).

Out of the specimens studied, PMO 235.659 shows the clearest triple-layered enameloid of all samples in this study. SCE, PBE and TBE are observed with distinct borders between the layers (Figure 17-3). The SCE only presents at the serrations at the base of the central cusp. The PBE-fibres are perpendicular to the serrations. The TBE appears as a thin layer at the base of the enameloid, and borders to the dentine. The triple-layer enameloid does not appear as clear closer to the apex, as they do further down on the crown shoulder. The triple-layered enameloid indicates a Neoselachii. The enameloid microstructures differ from *Grozonodon candaui* (Cuny et al., 1998) by the lack of radial bundles.

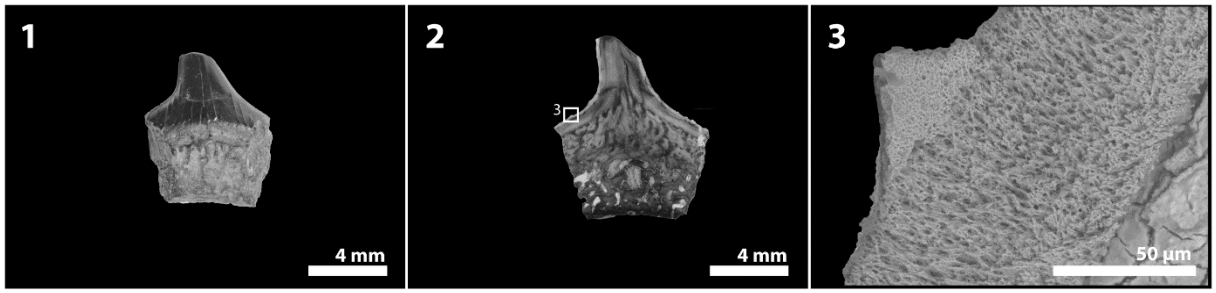

Figure 17 – *Grozonodon* sp.

PMO 235.659. 1, tooth in labial view; 2, thin section showing the dentinal histology; 3, SEM-image of the enameloid microstructures. SCE, PBE and TBE show as three well separated layers. The SCE is only present in the serrations, and shows no arranged crystallite structure. The PBE is the thickest layer and lies underneath the SCE. A thinner TBE is present at the base of the enameloid, and consists of haphazardly oriented bundles.

4. Discussion

4.1 Species determination

Determination of chondrichthyan species based on dental material is a task composed of observing morphology, dentinal histology and enameloid microstructures. To acquire the utmost certainty, a combination of all three features is preferred. However, concerning time and resources available, that is not always possible. In addition, the material used for histological examination often becomes destructed in the process.

Considering morphological features, some traits are more determining than others. For example, the number of lateral cusplets and crown ornamentation are unreliable criteria as they can vary a lot within the same species (Table 3). Klug et al. (2009) showed the heterogeneity and sexual dimorphism in the synechodontiform *Paraorthacodus jurensis*. There is a significant morphological variation between anterior and posterior teeth. Also, the difference in gender can be seen by the number of lateral cusplets, which Straube and Pollerspöck (2020) did a more recent study on. Crown ornamentation is uncertain as it can be worn down due to bad preservation, as seen in the *Synechodus incrementum* PMO 235.652. Still, not all morphological traits are unreliable. Root morphology is a good indicator. For Synechodontiformes the pseudopolyaulacorhize root vascularization pattern is a synapomorphy, and a labial root depression is common (Klug, 2010). Neoselachians as a whole, however, can possess different root vascularization patterns, as seen in *Grozonodon* sp. in this study (Figure 15). Again, not all specimens have a well-developed root vascularization pattern, making it harder to differentiate between the different types. Lastly, another feature that is more reliable for deciding taxa on species level is serrations (Türtscher et al., 2021).

Dentinal histology helps to support the possibility of synechodontiform taxa. Pseudoosteodonty is common in Synechodontiform sharks (Jambura et al., 2020). However, hybodonts, which share similar morphology to basal synechodontiforms have all three histotypes, including pseudoosteodont (Stumpf et al., 2021). Also, other Neoselachii taxa are not restricted to pseudoosteodonty (Jambura et al., 2020), so this feature is only helpful when determining synechodontiform taxa.

The most certain feature to evaluate when deciding taxa is enameloid microstructures. The parallel bundled enameloid (PBE) is a synapomorphy for neoselachians (Enault et al., 2015). Microstructures can also distinguish between genera as they do have some variations in whether

or not radial bundles are present (Andreev and Cuny, 2012). The durophagous hybodont *Acrodus cuneocostatus* have both a single crystallite enameloid (SCE) and one bundled enameloid layer (Cuny et al., 2001). This complicates the use of triple-layered enameloid as a criterion for Neoselachii. However, the morphology of *A. cuneocostatus* is completely different from the material studied in this project. Hybodonts that share morphological similarities to this project's material only have the SCE, so this does not affect the species determination of these neoselachian sharks.

As most chondrichthyan material from the fossil record consist of isolated teeth, the shark fauna may be overrepresented on species level. Considering the great variety that comes with heterogeneity, sexual dimorphism and ontogenesis (Purdy and Francis, 2007). Therefore, features like enameloid microstructures and root morphology are emphasized in this study.

4.1.1 Order Synechodontiformes – changes from the original description

Duffin and Ward (1993) were the first to describe the order Synechodontiformes, based on the three genera *Synechodus*, *Sphenodus* and *Paraortachodus*. They described the teeth as osteodont, however, Jambura et al. (2020) described the three Synechodontiform genera *Sphenodus*, *Paraorthacodus* and *Rhomphaiodon* as pseudoosteodont. All Synechodontiformes in this thesis exhibit the pseudoosteodont histotype.

Also, in the original description of Synechodontiformes Duffin and Ward (1993) described the root vascularization pattern as a modified anaulacorhize. A study by Klug (2010), that involved reexamination of the material from Klug and Kriwet (2008) and Klug et al. (2009), then concluded that all synechodontiforms possess the pseudopolyaulacorhize root vascularization pattern and a distinct labial root depression. The development of vascularization differs (Klug, 2010). This thesis is based on Klug (2010)'s determination of pseudopolyaulacorhize root vascularization together with the labial root depression as a synapomorphy.

4.1.2 *Synechodus incrementum*

Andreev and Cuny (2012) questioned the validity of *Synechodus incrementum* as both a *Synechodus* and even synechodontiform. They claimed that Johns et al. (1997) misinterpreted

the enameloid microstructures in their original description. What Johns et al. (1997) interpreted as parallel fibre bundles, Andreev and Cuny (2012) re-interpreted as single crystallite. Andreev and Cuny (2012) claimed that the parallel structures in the enameloid rather are a result of diagenesis, suggesting *S. incrementum* to have a hybodont enameloid. This study shows that *S. incrementum* undoubtedly possesses the neoselachian triple-layered enameloid (Figure 11), and supports Johns et al. (1997) interpretation. Together with the enameloid microstructures, and the pseudopolyaulacorhize root vascularization pattern, the positioning of *S. incrementum* in the genus *Synechodus* is supported.

PMO 235.661 and 235.665 has a significantly darker dentine than other studied samples. This might be due to their small size making a high cell density. In addition, 235.665 has a more dominating orthodentine and a less developed osteodentine.

PMO 235.652 does not have as prevalent crown ornamentation compared to PMO 235.661 and PMO 235.665. However, both the transverse crest and the apically radiating basal crests are present at the labial- and lingual face of the crown. This could be due to two different reasons; either it may have been worn down, or exposed to weathering during depositional processes.

4.1.3 *Rhomphaiodon*

Rhomphaiodon is a genus consisting of two species. Both of which are described in this project: *R. nicolensis* and *R. minor*. *Nemacanthus* fin spines are almost always found with *Rhomphaiodon* teeth (Cuny et al., 1998; Cuny and Risnes, 2005). Cuny and Risnes (2005) suggested that *Rhomphaiodon* and *Nemacanthus* belong to the same genus. No more fin spines are sorted out of the large material from the bonebed yet. However, Bratvold et al. (2018) described a *Nemacanthus* fin spine from the material gathered in 2015 from the Grippia level Bonebed. The findings of *Nemacanthus* together with *Rhomphaiodon* in the Grippia level Bonebed support Cuny and Risnes (2005)'s hypothesis of *Nemacanthus* and *Rhomphaiodon* to belong to the same genus.

4.1.4 *Grozonodon* sp. - Development of serrated cutting edges

The main features distinguishing *Grozonodon* sp. from the synechodontiforms in this study are the serrated cutting edges, as well as a different root vascularization pattern. Some of the teeth (e.g. *Synechodus* sp.) are described as having lateral cusplets that are more like an elevation of the crown. What distinguish this from the serrations is that serrations are primary enameloid structures, and they are a part of the occlusal crest (Moyer and Bemis, 2017; Türtscher et al., 2022). While lateral cusplets are a part of the crown as a whole and mainly consist of dentinal tissue with a thin enameloid layer on top. PMO 235.668 is a great example of this. Compared to the thin section of PMO 235.659, as seen in Figure 18 the difference between lateral cusplets and serrations becomes evident.

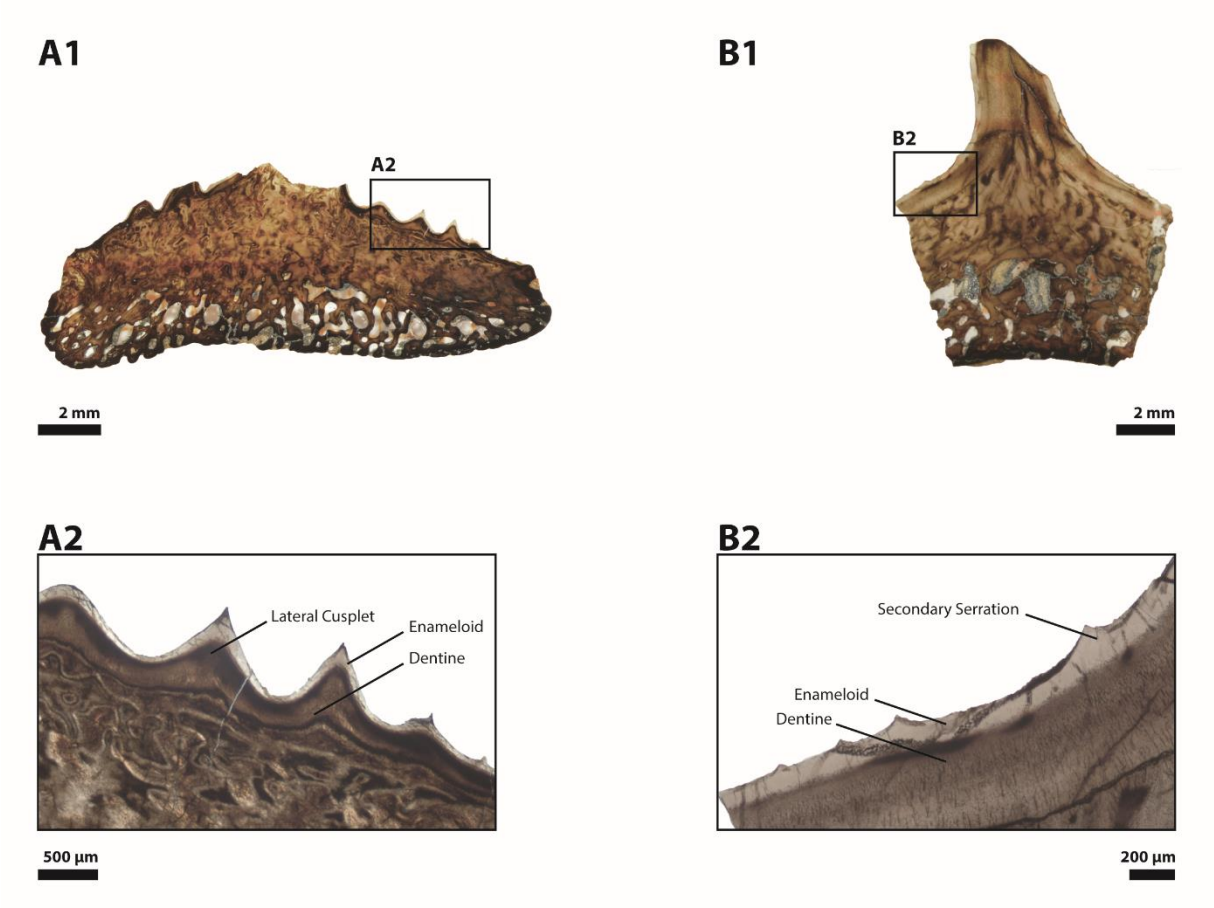

Figure 18 - Comparison of the tissues building up lateral cusplets and serrations. A1, Overview thin section of *Synechodus* sp. (PMO 235.668) parallel to the mesio-distal axis; A2, Close up of the thin section shows that the lateral cusplets are primarily consisting of dentinal tissue; B1, Overview thin section of *Grozonodon* sp. (PMO

235.659) parallel to the mesio-distal axis; B2, Close up of the thin section showing the serrated cutting edge. The serrations consist exclusively of enameloid.

The difference between primary and secondary serrations is that the primary serrations are partially filled with dentine, as opposed to secondary serrations that only consist of enameloid (Moyer and Bemis, 2017; Türtscher et al., 2022). Histological studies would therefore be necessary to decide the difference. Also, Moyer and Bemis (2017) stated that small serrations consist of SCE and PBE. PMO 235.659 and PMO 241.385 has secondary serrations (Moyer and Bemis, 2017) as they are only consisting of enameloid. Enameloid microstructures were only studied in one specimen, and only of the secondary serrations. The secondary serrations of the *Grozonodon* sp., PMO 235.659, consist of only SCE. Further studies on enameloid microstructures of PMO 241.470 would be necessary to comment on the histology of the primary serrations of *Grozonodon* sp.

Siversson and Machalski (2017) suggested that serrated cutting edges evolved in the Late Albian (Early Cretaceous). Andreev (2009) stated that serrated cutting edges developed in the family Anacoracidae of the lamniform sharks, also described from the Cretaceous. However, the finds of this study indicate a much earlier development of serrations. Even though the serrations are not particularly well developed, considering the shallow gullet, small size and the histology of them. This could represent a basal serration type.

A study on the extant Tiger Shark *Galeocerdo cuvier* by Türtscher et al. (2022) looked at ontogenetic and heterodonty variations of serrations. Their finds show that embryonic and juvenile teeth only exhibit less developed secondary serrations, while the adult specimens have developed primary serrations. Also, body size may interfere with the development of serrations, small-bodied sharks usually have secondary serrations (Türtscher et al., 2022). Moyer and Bemis (2017) hypothesized that histologically less complex secondary serrations are a plesimorphy from basal shark taxa, or a result of convergent evolution in selachians.

4.2 Variations in enameloid microstructures

For this project, enameloid microstructures were of great significance. The one trait that can indicate a Neoselachii with the most certainty is the triple-layered enameloid. Batomorphs and the Synechodontiform genera *Mucrovenator* and *Rhomaleodus* lack the TBE layer, making the

PBE layer synapomorphy for Neoselachii (Enault et al., 2015). Results have been varying, either in the sense of the presence of all three layers at once, or in the form of the ability to separate between layers. Only one of the observed species, *Synechodus* sp., exhibits radial bundles.

On all specimens, that exhibit the triple-layered enameloid, there were also part of the enameloid that appeared homogenous. The triple-layer was not present at all parts. Weathering can be a factor in this, but also the choice of studied section. The triple-layer is usually present where the enameloid is thickest (Enault et al., 2015), typically in the occlusal crest, apices, transverse crest, serrations or the apically oriented basal crests. PMO 235.661 is a good example of this (Figure 11). The SCE layer may be destructed under the etching process (Enault et al., 2015). This is also observed in PMO 235.659, which has only sparse remains of the SCE layer (Figure 19). The BCE unit is however present all over. Since it is the PBE that is the synapomorphy, it can still be concluded that the specimen has the Neoselachii triple-layer, even though not all layers are observed. However when the enameloid appears homogenous it is not that easy to say if it is SCE of a hybodont or PBE, it is easier to spot the difference when you have both types present.

The enameloid microstructures are more complex at the apex of the crown than at the base (Cuny and Risnes, 2005). Meaning sections parallel to the mesio-distal- or the apico-basal plane are preferred when studying enameloid microstructures. Sections taken parallel to the lingo-labial plane, or specimens with a broken apex should therefore be carefully interpreted. Out of the four *Synechodus* sp. that were studied in SEM, PMO 235.656 was the only one where radial bundles were not observed (Figure 9). PMO 235.656 was studied in the lingo-labial plane. Taking into account the difficulties of studying enameloid microstructures, PMO 235.656 was still determined to be *Synechodus* sp. based on the other morphological features.

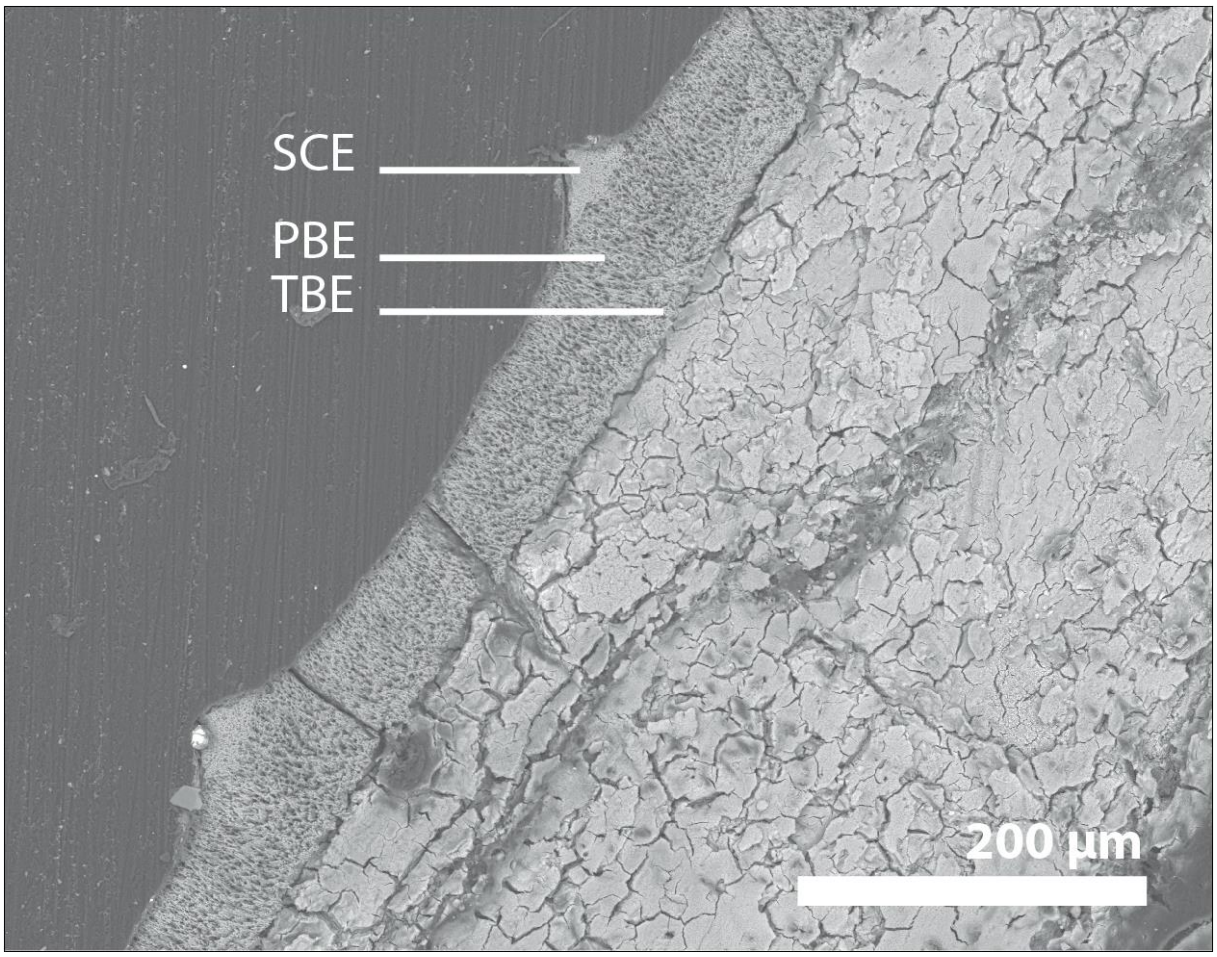

Figure 19 - Enameloid microstructures of the serrated cutting edge of *Grozonodon* sp. (PMO 235.659). Abbreviations: PBE, Parallel bundled enameloid; SCE, Single crystallite enameloid; TBE, Tangled bundled enameloid.

The radial bundles are previously thought to first have developed in the Middle/Late Triassic and are an indication of a derived PBE. PBE without radial bundles is seen as a primitive trait (Andreev and Cuny, 2012). *Synechodus* sp. is the only species that has radial bundles. Compared to the other taxa described in this study *Synechodus* sp. has the most derived enameloid. This indicates an earlier development of radial bundles.

4.3 Comparison of SEM-, CT- and microscopy imaging

This project uses three different methods for imaging of histological data. Scanning electron microscopy (SEM), computed tomography (CT) and a standard microscope. When looking at enameloid microstructures, SEM-imaging of etched teeth gives the best results. However, the TBE is possible to observe in the thin sections, which indicates the presence of a triple-layered

enameloid. Even though it is the PBE, and not the TBE, that is the synapomorphy for neoselachians, the presence of TBE without PBE has not been recorded. The TBE is after all a more derived enameloid tissue (Andreev and Cuny, 2012), and it is, therefore, reasonable to presume the presence of PBE based on TBE observations. While with CT-imaging it is not possible to see structures within the enameloid at all. CT-imaging is a good choice for bigger histological examination, e.g. dentinal tissue. It gives a three dimensional view of the whole tooth and it is possible to see how the different tissues interact with each other. The advantage of CT-scanning is that the material does not get damaged at all, as opposed to etching and sectioning for SEM or making thin sections.

PMO 235.652 and PMO 235.654 did not have remaining material after sectioning for SEM, but when comparing the thin sections to that of PMO 235.661, the dark fibred structures in the enameloid could represent the TBE (Figure 20). PMO 235.665 has the same fibres shown in the thin section, and when looking at it etched in SEM it is without doubt TBE. A study by Moyer and Bemis (2017) showed thin sections of extant sharks, where enameloid microstructures are visible. If the dark fibres in the apex of PMO 235.652 are TBE, PMO 235.652 is *Synechodus incrementum.* PMO 235.654 is too poorly preserved to decide taxa with certainty, possible *Grozonodon,* but no serrations are found in the little that is left of the material. There is a strong transverse crest on the lingual side and strong crown-basal apically oriented crests, otherwise the crown is smooth. Root vascularization pattern is not available. Based on this, the placement of PMO 235.654 within *Grozonodon* sp. is of great uncertainty.

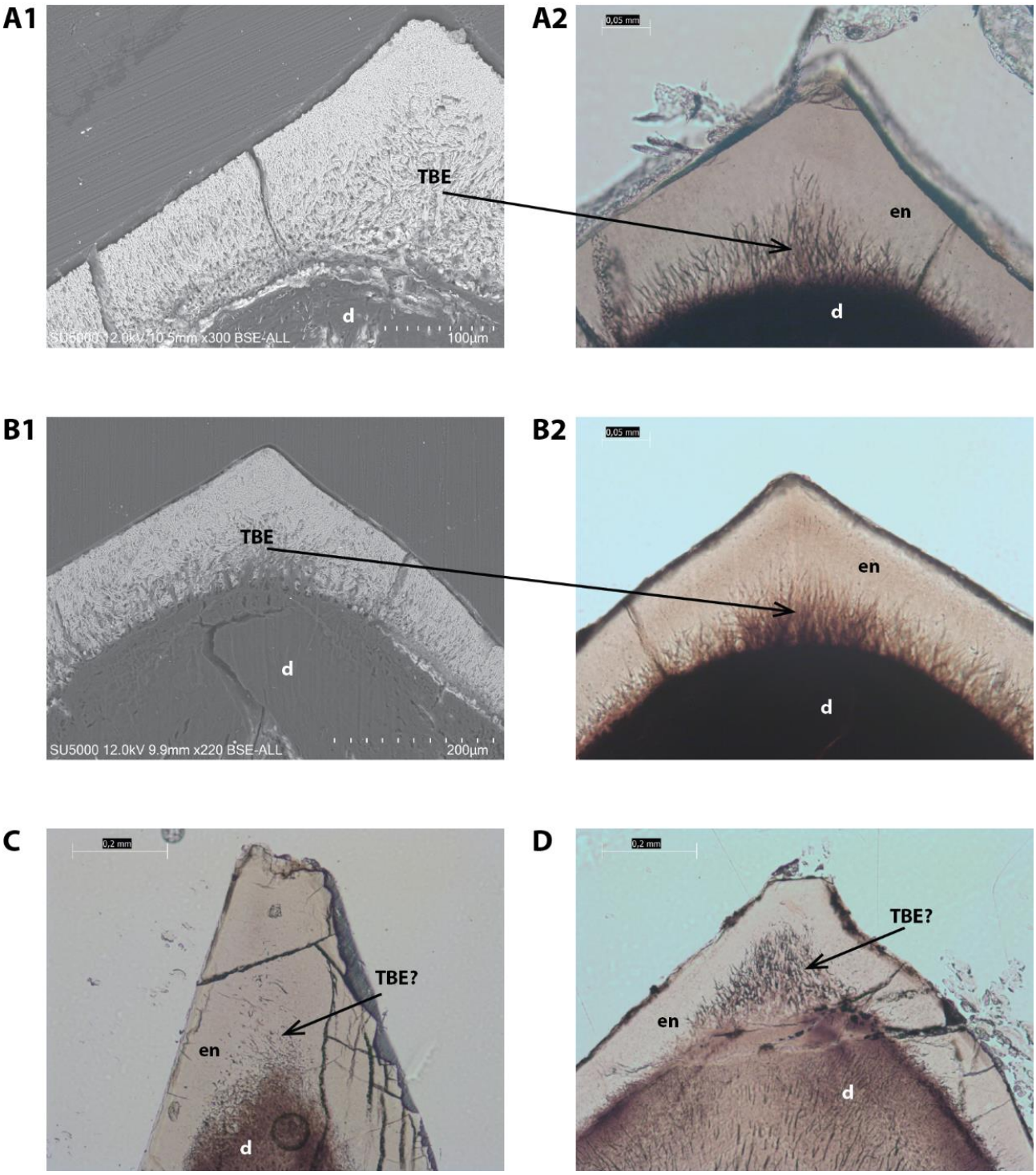

Figure 20 - A1, PMO 235.661 in SEM; A2, Thin Section of PMO 235.661; B1, PMO 235.665 in SEM; B2, Thin section of PMO 235.665; C, Thin section of PMO 235.654; D, Thin Section of PMO 235.652. Arrows show the corresponding area from SEM-image to the thin section. All thin sections are showing the apex perpendicular to the mesio-distal axis. Abbreviations: d, Dentine; en, Enameloid; TBE, Tangled bundled enameloid.

4.4 Chondrichthyans in the Grippia level Bonebed

Table 4 - Chondrichthyans described from the Grippia level Bonebed (Stensiö, 1921; Cox and Smith, 1973; Bratvold et al., 2018). Showing added taxa from Bratvold et al. (2018) and from this study (2016 material). X, Present; -, Not present; Na, Not available. Modified from Bratvold et al. (2018).

Horizon	Formation	Chondrichthyan taxa	2015 material Bratvold et. al. (2018)	2016 material
Grippia 'niveau'	Vikinghøgda Fm.	*Acrodus scaber*	X	Na
		Acrodus spitzbergensis	X	Na
		Acrodus vermiformis	-	Na
		Hybodus microdus	X	Na
		Hybodus rapax	X	Na
		Lissodus angulatus	X	Na
		Nemacanthus sp.	X	Na
		Palaeobates sp.	*Palaeobates polaris*	Na
			Acrodus gaillardoti	Na
		Unsure (Stensiö, 1921)	*Acrodus oppenheimeri*	Na
			Acrodus lateralis	Na
			Acrodus sp.	Na
			Hybodus sasseniensis	Na
			Polyacrodus sp.	Na
			Synechodontiform sp. (1)	*Grozonodon* sp.
				Rhomphaiodon minor
				Rhomphaiodon nicolensis
			Synechodontiform sp. (2)	*Synechodus incrementum*
				Synechodus sp.

Bratvold et al. (2018) identified seven genera and 15 species from the Grippia level Bonebed (Table 4). Many of them are known from previous descriptions (Stensiö, 1921; Cox and Smith, 1973), eight of them have not been described from the bonebed earlier. The material from 2016, described in this thesis, contributes to an addition of three genera and five species to the Grippia level Bonebed. All of them belong to the Neoselachii group. The two synechodontiforms described by Bratvold et al. (2018) were identified as *Synechodus incrementum* (Synechodontiform sp. 2) and the Neoselachii *Grozonodon* (Synechodontiform sp. 1, PMO 230.110 and PMO 230.129). As this thesis only focused on neoselachian teeth, all other material have not been regarded.

4.5 Early evolution of Neoselachian sharks

Hybodonts, which are considered a sister group to neoselachians (Maisey et al., 2004; Andreev and Cuny, 2012), appeared in the Devonian (Hairapetian and Ginter, 2009; Andreev and Cuny, 2012). Based on this Andreev and Cuny (2012) inferred that it is likely that the neoselachians appeared during the same time.

The earliest described Neoselachii is *Synechodus antiquus* from the Early Permian of Russia (Ivanov, 2005). However, the well-defined triple-layered enameloid was first proved by Johns et al. (1997) in three *Synechodus* species from the Late Triassic (Carnian). With the results from this study, a well-defined triple-layered enameloid is proven in *Synechodus incrementum, Rhomphaiodon minor, Rhomphaiodon nicolensis* and *Grozonodon* sp. in addition, radial bundles in *Synechodus* sp. from the Early Triassic (Spathian).

4.6 Biogeography

In the Early Triassic the world consisted of the supercontinent Pangaea and four main seas; Boreal, Panthalassa, Neotethys and Palaeotethys (Figure 21). Spitsbergen was situated in the Boreal Sea (Koot, 2013). *Grozonodon, Rhomphaiodon minor, Rhomphaiodon nicolensis* and *Synechodus incrementum* are taxa that already are described from the same region, that being Boreal Sea (France, England, Belgium, Germany) and East-Panthalassa (British Columbia of Canada) (Johns et al., 1997; Cuny et al., 1998; Cuny and Risnes, 2005; Sander et al., 2016). *Synechodus* as a genus is the most widespread out of the taxa described, in addition to the Boreal

Sea (Cuny and Risnes, 2005), Yamagishi (2004) described *Synechodus* from the Mid Panthalassa (Japan) (Figure 21).

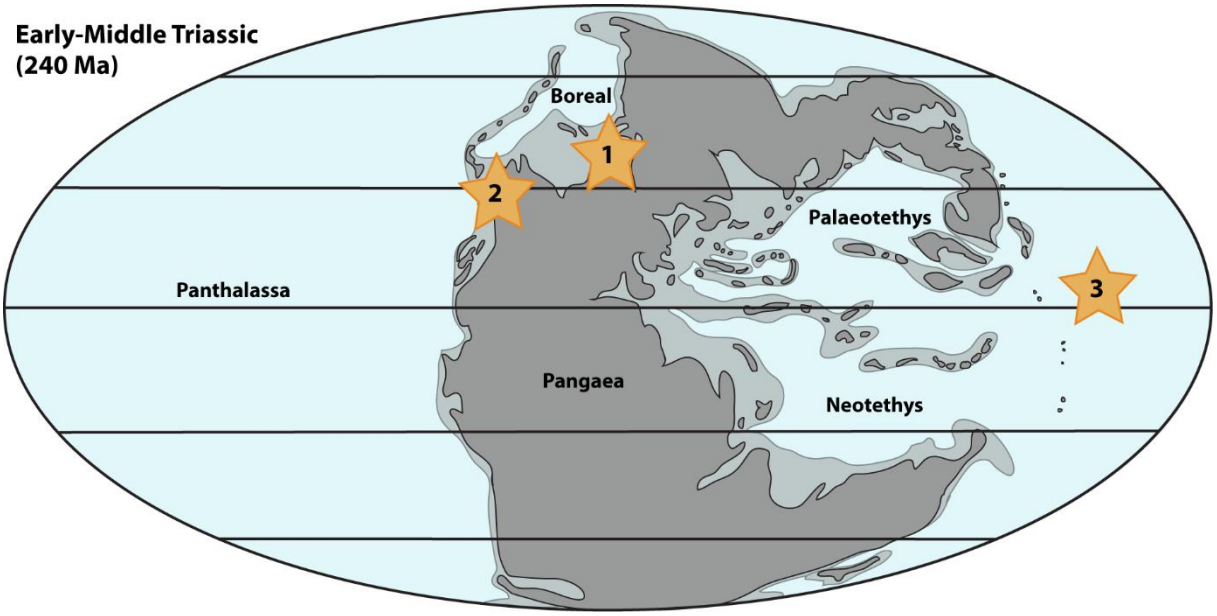

Figure 21 – Map of the Early-Middle Triassic World (240 million years ago). The stars represent other findings of the species described in this study, 1, Spitsbergen, France, Belgium; Germany; 2, British Columbia; 3, Japan. Redrawn and modified from Koot (2013).

4.7 The future for Chondrichthyans

The crown-chondrichthyans, which are represented by extant species today, survived all four mass extinction events since their first appearance in the Devonian (Miller et al., 2003). In addition, they are considered one of the more successful survivors of the PTME (Koot, 2013).

Today at least one-third of all chondrichthyans are threatened with extinction (Turner, 2021). Overfishing makes the biggest threat (Dulvy et al., 2021), however, loss of habitat, pollution and climate change also contributes to the problem (Turner, 2021). Maintaining apex predators in ecosystems keep the ecosystem stable, and without predators there will be further loss of biodiversity (Scheyer et al., 2014).

5. Conclusions

This thesis concludes that:

1. Five species, within three genera of Neoselachii teeth, are now described from the Grippia level Bonebed of Spitsbergen, Norway. Four of them are in the order Synechodontiformes. Two of them, *Synechodus* sp. and *Grozonodon* sp. are not referable to any other species, and thus this suggests two new species of neoselachian sharks.

2. For species determination of Neoselachii teeth, a combination of enameloid microstructures and root morphology is preferred, as crown morphology varies due to heterogeneity, sexual dimorphism and ontogenesis.

3. Basal serrations found on *Grozonodon* sp. indicate a much earlier development of serrations than previously stated.

4. The findings of a well-defined triple-layer in all described species and the additional radial bundles in *Synechodus* sp. give proof to the development of the neoselachian enameloid in the Early Triassic, as opposed to the previous first description from the Late Triassic.

References

ANDREEV, P. S. 2009. Enameloid microstructure of the serrated cutting edges in certain fossil carcharhiniform and lamniform sharks. *Microscopy Research and Technique***,** NA-NA.

ANDREEV, P. S., COATES, M. I., KARATAJŪTĖ-TALIMAA, V., SHELTON, R. M., COOPER, P. R., WANG, N.-Z. & SANSOM, I. J. 2016. The systematics of the Mongolepidida (Chondrichthyes) and the Ordovician origins of the clade. *PeerJ,* 4**,** e1850.

ANDREEV, P. S., COATES, M. I., SHELTON, R. M., COOPER, P. R., SMITH, M. P. & SANSOM, I. J. 2015. Upper Ordovician chondrichthyan-like scales from North America. *Palaeontology,* 58**,** 691-704.

ANDREEV, P. S. & CUNY, G. 2012. New Triassic stem selachimorphs (Chondrichthyes, Elasmobranchii) and their bearing on the evolution of dental enameloid in Neoselachii. *Journal of Vertebrate Paleontology,* 32**,** 255-266.

BARNOSKY, A. D., MATZKE, N., TOMIYA, S., WOGAN, G. O. U., SWARTZ, B., QUENTAL, T. B., MARSHALL, C., MCGUIRE, J. L., LINDSEY, E. L., MAGUIRE, K. C., MERSEY, B. & FERRER, E. A. 2011. Has the Earth's sixth mass extinction already arrived? *Nature,* 471**,** 51-57.

BATCHELOR, T. J. & DUFFIN, C. J. 2020. First description of sharks' teeth from the Ferruginous Sands Formation (Aptian, Early Cretaceous) of the Isle of Wight. *Proceedings of the Geologists' Association,* 131**,** 353-359.

BENTON, M. J. 1987. Progress and competition in macroevolution. *Biological Reviews,* 62**,** 305-338.

BERNARDI, M., PETTI, F. M. & BENTON, M. J. 2018. Tetrapod distribution and temperature rise during the Permian–Triassic mass extinction. *Proceedings of the Royal Society B: Biological Sciences,* 285**,** 20172331.

BIRKENMAJER, K. & JERZMAŃSKA, A. 1979. Lower Triassic shark and other fish teeth from Hornsund, south Spitsbergen. *Studia Geologica Polonica,* 60**,** 7-37.

BŁAŻEJOWSKI, B. 2004. Shark teeth from the Lower Triassic of Spitsbergen and their histology. *Polish Polar Research***,** 153-167-153-167.

BOISVERT, C. A., JOHNSTON, P., TRINAJSTIC, K. & JOHANSON, Z. 2019. Chondrichthyan Evolution, Diversity, and Senses. Springer International Publishing.

BONAPARTE, C. L. 1838. *Synopsis vertebratorum systematis,* Nuovi Annali delle Naturali (Bologna).

BRATVOLD, J., DELSETT, L. L. & HURUM, J. H. 2018. Chondrichthyans from the Grippia bonebed (Early Triassic) of Marmierfjellet, Spitsbergen. *Norsk Geologisk Tidsskrift,* 98**,** 189-217.

BRAZEAU, M. D. & FRIEDMAN, M. 2014. The characters of Palaeozoic jawed vertebrates. *Zoological Journal of the Linnean Society,* 170**,** 779-821.

BRAZEAU, M. D. & FRIEDMAN, M. 2015. The origin and early phylogenetic history of jawed vertebrates. *Nature,* 520**,** 490-497.

BUCHAN, S., CHALLINOR, A., HARLAND, W. & PARKER, J. 1965. The Triassic stratigraphy of Svalbard.

BURGESS, S. D., MUIRHEAD, J. D. & BOWRING, S. A. 2017. Initial pulse of Siberian Traps sills as the trigger of the end-Permian mass extinction. *Nature Communications,* 8.

CARRILLO-BRICEÑO, J. D., CADENA, E. A., DECECCHI, A. T., LARSON, H. C. & DU, T. Y. 2016. First record of a hybodont shark (Chondrichthyes: Hybodontiformes) from the Lower Cretaceous of Colombia. *Neotropical Biodiversity,* 2**,** 81-86.

CEBALLOS, G., EHRLICH, P. R., BARNOSKY, A. D., GARCÍA, A., PRINGLE, R. M. & PALMER, T. M. 2015. Accelerated modern human–induced species losses: Entering the sixth mass extinction. *Science advances,* 1**,** e1400253.

CEBALLOS, G., EHRLICH, P. R. & DIRZO, R. 2017. Biological annihilation via the ongoing sixth mass extinction signaled by vertebrate population losses and declines. *Proceedings of the National Academy of Sciences,* 114**,** E6089-E6096.

CEBALLOS, G., EHRLICH, P. R. & RAVEN, P. H. 2020. Vertebrates on the brink as indicators of biological annihilation and the sixth mass extinction. *Proceedings of the National Academy of Sciences,* 117**,** 13596-13602.

COATES, M. I., FINARELLI, J. A., SANSOM, I. J., ANDREEV, P. S., CRISWELL, K. E., TIETJEN, K., RIVERS, M. L. & LA RIVIERE, P. J. 2018. An early chondrichthyan and the evolutionary assembly of a shark body plan. *Proceedings of the Royal Society B: Biological Sciences,* 285**,** 20172418.

COHEN, K. M., FINNEY, S. C., GIBBARD, P. L. & FAN, J.-X. 2013. The ICS international chronostratigraphic chart. *Episodes,* 36**,** 199-204.

COX, C. & SMITH, D. G. 1973. A review of the Triassic vertebrate faunas of Svalbard. *Geological Magazine,* 110**,** 405-418.

CUNY, G. & BENTON, M. J. 1999. Early radiation of the Neoselachian sharks in Western Europe. *Geobios,* 32**,** 193-204.

CUNY, G., HUNT, A., MAZIN, J.-M. & RAUSCHER, R. 2000. Teeth of enigmatic neoselachian sharks and an ornithischian dinosaur from the uppermost Triassic of Lons-le-Saunier (Jura, France). *Paläontologische Zeitschrift,* 74**,** 171-185.

CUNY, G., MARTIN, M., RAUSCHER, R. & MAZIN, J.-M. 1998. A new neoselachian shark from the Upper Triassic of Grozon (Jura, France). *Geological Magazine,* 135**,** 657-668.

CUNY, G., RIEPPEL, O. & SANDER, P. M. 2001. The shark fauna from the Middle Triassic (Anisian) of north-western Nevada. *Zoological Journal of the Linnean Society,* 133**,** 285-301.

CUNY, G. & RISNES, S. 2005. The enameloid microstructure of the teeth of synechodontiform sharks (Chondrichthyes: Neoselachii). *PalArch's Journal of Vertebrate Palaeontology,* 3**,** 1-19.

DEAN, M. N. & SUMMERS, A. P. 2006. Mineralized cartilage in the skeleton of chondrichthyan fishes. *Zoology,* 109**,** 164-168.

DEARDEN, R. P., BLAAUWEN, J. L., SANSOM, I. J., BURROW, C. J., DAVIDSON, R. G., NEWMAN, M. J., KO, A. & BRAZEAU, M. D. 2021. A revision of Vernicomacanthus Miles with comments on the characters of stem-group chondrichthyans. *Papers in Palaeontology,* 7**,** 1949-1976.

DUFFIN, C. & WARD, D. 1993. The Early Jurassic palaeospinacid sharks of Lyme Regis, southern England. *Professional Paper. Geological Survey of Belgium*.

DULVY, N. K., PACOUREAU, N., RIGBY, C. L., POLLOM, R. A., JABADO, R. W., EBERT, D. A., FINUCCI, B., POLLOCK, C. M., CHEOK, J., DERRICK, D. H., HERMAN, K. B., SHERMAN, C. S., VANDERWRIGHT, W. J., LAWSON, J. M., WALLS, R. H. L., CARLSON, J. K., CHARVET, P., BINEESH, K. K., FERNANDO, D., RALPH, G. M., MATSUSHIBA, J. H., HILTON-TAYLOR, C., FORDHAM, S. V. & SIMPFENDORFER, C. A. 2021. Overfishing drives over one-third of all sharks and rays toward a global extinction crisis. *Current Biology*.

ENAULT, S., GUINOT, G., KOOT, M. B. & CUNY, G. 2015. Chondrichthyan tooth enameloid: past, present, and future. *Zoological Journal of the Linnean Society,* 174**,** 549-570.

GUINOT, G., ADNET, S., CAVIN, L. & CAPPETTA, H. 2013. Cretaceous stem chondrichthyans survived the end-Permian mass extinction. *Nature communications,* 4**,** 1-8.

GUINOT, G. & CAPPETTA, H. 2011. Enameloid microstructure of some Cretaceous Hexanchiformes and Synechodontiformes (Chondrichthyes, Neoselachii): new structures and systematic implications. *Microscopy Research and Technique,* 74**,** 196-205.

HAIRAPETIAN, V. & GINTER, M. 2009. Famennian chondrichthyan remains from the Chahriseh section, central Iran. *Acta Geologica Polonica,* 59**,** 173-200.

HAMMER, Ø., JONES, M. T., SCHNEEBELI-HERMANN, E., HANSEN, B. B. & BUCHER, H. 2019. Are Early Triassic extinction events associated with mercury anomalies? A reassessment of the Smithian/Spathian boundary extinction. *Earth-Science Reviews,* 195**,** 179-190.

HANSEN, B. B., HAMMER, Ø. & NAKREM, H. A. 2018. Stratigraphy and age of the Grippia niveau bonebed, Lower Triassic Vikinghøgda Formation, Spitsbergen. *Norsk Geologisk Tidsskrift,* 98**,** 175-187.

HEINICKE, M., NAYLOR, G. & HEDGES, S. 2009. Cartilaginous fishes (Chondrichthyes). *The timetree of life,* 9**,** 320-7.

HEROLD, R., ROSENBLOOM, J. & GRANOVSKY, M. 1989. Phylogenetic distribution of enamel proteins: immunohistochemical localization with monoclonal antibodies indicates the evolutionary appearance of enamelins prior to amelogenins. *Calcified tissue international,* 45**,** 88-94.

HULKE, J. W. 1873. *Memorandum on some fossil vertebrate remains collected by the Swedish expeditions to Spitzbergen in 1864 and 1868,* PA Norstedt & Söner.

HURUM, J. H., ENGELSCHIØN, V. S., ØKLAND, I. H., BRATVOLD, J., EKEHEIEN, C., ROBERTS, A. J., DELSETT, L. L., HANSEN, B. B., MØRK, A. & NAKREM, H. A. 2018. The history of exploration and stratigraphy of the Early to Middle Triassic vertebrate-bearing strata of Svalbard (Sassendalen Group, Spitsbergen). *Norwegian Journal of Geology,* 98**,** 165-174.

HUTCHINGS, J. A., MYERS, R. A., GARCÍA, V. B., LUCIFORA, L. O. & KUPARINEN, A. 2012. Life-history correlates of extinction risk and recovery potential. *Ecological Applications,* 22**,** 1061-1067.

IVANOV, A. 2005. Early Permian chondrichthyans of the middle and south Urals. *Revista Brasileira de Paleontologia,* 8**,** 127-138.

JAMBURA, P. L., TÜRTSCHER, J., KINDLIMANN, R., METSCHER, B., PFAFF, C., STUMPF, S., WEBER, G. W. & KRIWET, J. 2020. Evolutionary trajectories of tooth histology patterns in modern sharks (Chondrichthyes, Elasmobranchii). *Journal of Anatomy,* 236**,** 753-771.

JOACHIMSKI, M. M., LAI, X., SHEN, S., JIANG, H., LUO, G., CHEN, B., CHEN, J. & SUN, Y. 2012. Climate warming in the latest Permian and the Permian-Triassic mass extinction. *Geology,* 40**,** 195-198.

JOHNS, M. J., BARNES, C. R. & ORCHARD, M. J. 1997. *Taxonomy and biostratigraphy of Middle and Late Triassic elasmobranch ichthyoliths from northeastern British Columbia*, Geological Survey of Canada.

KLUG, S. 2009. Synechodontiformes, a largely disregarded group of early modern sharks in the Jurassic. *Actes 2009 bis***,** 50.

KLUG, S. 2010. Monophyly, phylogeny and systematic position of the† Synechodontiformes (Chondrichthyes, Neoselachii). *Zoologica scripta,* 39**,** 37-49.

KLUG, S. & KRIWET, J. 2008. A new basal galeomorph shark (Synechodontiformes, Neoselachii) from the Early Jurassic of Europe. *Naturwissenschaften,* 95**,** 443-448.

KLUG, S., KRIWET, J., BOETTCHER, R., SCHWEIGERT, G. & DIETL, G. 2009. Skeletal anatomy of the extinct shark Paraorthacodus jurensis (Chondrichthyes; Palaeospinacidae), with comments on synechodontiform and palaeospinacid monophyly. *Zoological Journal of the Linnean Society,* 157**,** 107-134.

KOOT, M. B. 2013. Effects of the Late Permian mass extinction on chondrichthyan palaeobiodiversity and distribution patterns.

KOOT, M. B., CUNY, G., ORCHARD, M. J., RICHOZ, S., HART, M. B. & TWITCHETT, R. J. 2015. New hybodontiform and neoselachian sharks from the Lower Triassic of Oman. *Journal of Systematic Palaeontology,* 13**,** 891-917.

KRIWET, J., KIESSLING, W. & KLUG, S. 2009. Diversification trajectories and evolutionary life-history traits in early sharks and batoids. *Proceedings of the Royal Society B: Biological Sciences,* 276**,** 945-951.

LI, G., LIAO, W., LI, S., WANG, Y. & LAI, Z. 2021. Different triggers for the two pulses of mass extinction across the Permian and Triassic boundary. *Scientific Reports,* 11**,** 1-12.

LUND, R. & GROGAN, E. D. 1997. Relationships of the Chimaeriformes and the basal radiation of the Chondrichthyes. *Reviews in Fish Biology and Fisheries,* 7**,** 65-123.

MAISEY, J. G., DENTON, J. S. S., BURROW, C. & PRADEL, A. 2021. Architectural and ultrastructural features of tessellated calcified cartilage in modern and extinct chondrichthyan fishes. *Journal of Fish Biology,* 98**,** 919-941.

MAISEY, J. G., NAYLOR, G. J. & WARD, D. 2004. Mesozoic elasmobranchs, neoselachian phylogeny and the rise of modern elasmobranch diversity. *Mesozoic fishes,* 3**,** 17-56.

MANZANARES UBEDA, E. 2020. Chondrichthyans from the Spanish Triassic (westernmost Tethys) with remarks on the evolution of enameloid.

MIAKE, Y., AOBA, T., MORENO, E., SHIMODA, S., PROSTAK, K. & SUGA, S. 1991. Ultrastructural studies on crystal growth of enameloid minerals in elasmobranch and teleost fish. *Calcified tissue international,* 48**,** 204-217.

MILLER, R. F., CLOUTIER, R. & TURNER, S. 2003. The oldest articulated chondrichthyan from the Early Devonian period. *Nature,* 425**,** 501-504.

MOYER, J. K. & BEMIS, W. E. 2017. Shark teeth as edged weapons: serrated teeth of three species of selachians. *Zoology,* 120**,** 101-109.

MØRK, A., ELVEBAKK, G., FORSBERG, A. W., HOUNSLOW, M. W., NAKREM, H. A., VIGRAN, J. O. & WEITSCHAT, W. 1999. The type section of the Vikinghogda Formation: a new Lower Triassic unit in central and eastern Svalbard. *Polar research,* 18**,** 51-82.

PURDY, R. W. & FRANCIS, M. P. 2007. Ontogenetic development of teeth in Lamna nasus (Bonnaterre, 1758)(Chondrichthyes: Lamnidae) and its implications for the study of fossil shark teeth. *Journal of Vertebrate Paleontology,* 27**,** 798-810.

RADINSKY, L. 1961. Tooth histology as a taxonomic criterion for cartilaginous fishes. *Journal of Morphology,* 109**,** 73-92.

RAUP, D. M. 1979. Size of the Permo-Triassic Bottleneck and Its Evolutionary Implications. *Science,* 206**,** 217-218.

RAUP, D. M. & SEPKOSKI, J. J., JR 1982. Mass extinctions in the marine fossil record. *Science,* 215**,** 1501-1503.

REGAN, C. T. 1906. *A classification of the selachian fishes*, Proceedings of the Zoological Society of London 1906.

ROMANO, C., ARGYRIOU, T. & KRUMENACKER, L. J. 2019. Chondrichthyan teeth from the Early Triassic Paris Biota (Bear Lake County, Idaho, USA). *Geobios,* 54**,** 63-70.

ROMANO, C. & BRINKMANN, W. 2010. A new specimen of the hybodont shark Palaeobates polaris with three-dimensionally preserved Meckel's cartilage from the Smithian (Early Triassic) of Spitsbergen. *Journal of Vertebrate Paleontology,* 30**,** 1673-1683.

ROMANO, M., BERNARDI, M., PETTI, F. M., RUBIDGE, B., HANCOX, J. & BENTON, M. J. 2020. Early Triassic terrestrial tetrapod fauna: a review. *Earth-Science Reviews***,** 103331.

RÜCKLIN, M., KING, B., CUNNINGHAM, J. A., JOHANSON, Z., MARONE, F. & DONOGHUE, P. C. J. 2021. Acanthodian dental development and the origin of gnathostome dentitions. *Nature Ecology & Evolution,* 5**,** 919-926.

SANDER, P. M., WINTRICH, T., SCHWERMANN, A. H. & KINDLIMANN, R. 2016. Die paläontologische Grabung in der Rhät-Lias-Tongrube der Fa. Lücking bei Warburg-Bonenburg (Kr. Höxter) im Frühjahr 2015. *Geologie und Paläontologie in Westfalen,* 88**,** 11-37.

SCHEYER, T. M., ROMANO, C., JENKS, J. & BUCHER, H. 2014. Early Triassic Marine Biotic Recovery: The Predators' Perspective. *PLoS ONE*, 9**,** e88987.

SEPKOSKI, J. J., JR 1986. Phanerozoic overview of mass extinction. *Patterns and Processes in the History of Life.* Springer.

SIVERSSON, M. & MACHALSKI, M. 2017. Late late Albian (Early Cretaceous) shark teeth from Annopol, Poland. *Alcheringa: An Australasian Journal of Palaeontology,* 41**,** 433-463.

SMITH, M. & SANSOM, I. 2000. *Evolutionary origins of dentine in the fossil record of early vertebrates: diversity, development and function,* Cambridge University Press Cambridge.

SONG, H., WIGNALL, P. B., TONG, J. & YIN, H. 2013. Two pulses of extinction during the Permian–Triassic crisis. *Nature Geoscience,* 6**,** 52-56.

STANLEY, S. M. 2016. Estimates of the magnitudes of major marine mass extinctions in earth history. *Proc Natl Acad Sci U S A,* 113**,** E6325-E6334.

STENSIÖ, E. A. 1918. *Notes on some fish remains collected at Hornsund by the Norwegian Spitzbergen Expedition in 1917*.

STENSIÖ, E. A. 1921. *Triassic fishes from Spitzbergen,* A. Holzhausen.

STRAUBE, N. & POLLERSPÖCK, J. 2020. Intraspecific dental variations in the deep-sea shark Etmopterus spinax and their significance in the fossil record. *Zoomorphology,* 139**,** 483-491.

STUMPF, S., LÓPEZ-ROMERO, F. A., KINDLIMANN, R., LACOMBAT, F., POHL, B. & KRIWET, J. 2021. A unique hybodontiform skeleton provides novel insights into Mesozoic chondrichthyan life. *Papers in Palaeontology,* 7**,** 1479-1505.

TILMAN, D., CLARK, M., WILLIAMS, D. R., KIMMEL, K., POLASKY, S. & PACKER, C. 2017. Future threats to biodiversity and pathways to their prevention. *Nature,* 546**,** 73-81.

TURNER, M. 2021. Chondrichthyan crisis. *Nature Ecology & Evolution,* 5**,** 1471-1471.

TÜRTSCHER, J., JAMBURA, P. L., LÓPEZ-ROMERO, F. A., KINDLIMANN, R., SATO, K., TOMITA, T. & KRIWET, J. 2022. Heterodonty and ontogenetic shift dynamics in the dentition of the tiger shark *Galeocerdo cuvier* (Chondrichthyes, Galeocerdidae). *Journal of Anatomy*.

TÜRTSCHER, J., LÓPEZ-ROMERO, F. A., JAMBURA, P. L., KINDLIMANN, R., WARD, D. J. & KRIWET, J. 2021. Evolution, diversity, and disparity of the tiger shark lineage Galeocerdo in deep time. *Paleobiology,* 47**,** 574-590.

UNDERWOOD, C. J. 2006. Diversification of the Neoselachii (Chondrichthyes) during the Jurassic and Cretaceous. *Paleobiology,* 32**,** 215-235.

VÁZQUEZ, P. & CLAPHAM, M. E. 2017. Extinction selectivity among marine fishes during multistressor global change in the end-Permian and end-Triassic crises. *Geology,* 45**,** 395-398.

WIGNALL, P. B. & TWITCHETT, R. J. 1996. Oceanic anoxia and the end Permian mass extinction. *Science,* 272**,** 1155-1158.

WILLIAMS, D. R., CLARK, M., BUCHANAN, G. M., FICETOLA, G. F., RONDININI, C. & TILMAN, D. 2021. Proactive conservation to prevent habitat losses to agricultural expansion. *Nature Sustainability,* 4**,** 314-322.

WIMAN, C. 1929. Eine neue reptilien-ordnung aus der Trias Spitzbergens. *Bulletin of the Geological Institution of the University of Upsala,* 22**,** 183-196.

WOODWARD, A. S. 1889. *Catalogue of the Fossil Fishes in the British Museum (Natural History): Elasmobranchii*, order of the Trustees.

WU, Y., CHU, D., TONG, J., SONG, H., DAL CORSO, J., WIGNALL, P. B., SONG, H., DU, Y. & CUI, Y. 2021. Six-fold increase of atmospheric p CO 2 during the Permian–Triassic mass extinction. *Nature communications,* 12**,** 1-8.

YAMAGISHI, H. 2004. Elasmobranch remains from the Taho limestone (lower-Middle Triassic) of Ehime prefecture, Southwest Japan. *Mesozoic fishes,* 3**,** 565-574.

YIN, H., JIANG, H., XIA, W., FENG, Q., ZHANG, N. & SHEN, J. 2014. The end-Permian regression in South China and its implication on mass extinction. *Earth-Science Reviews,* 137**,** 19-33.

YIN, H. & SONG, H. 2013. Mass extinction and Pangea integration during the Paleozoic-Mesozoic transition. *Science China Earth Sciences,* 56**,** 1791-1803.

ZHU, M., ZHAO, W., JIA, L., LU, J., QIAO, T. & QU, Q. 2009. The oldest articulated osteichthyan reveals mosaic gnathostome characters. *Nature,* 458**,** 469-474.

Appendix

Appendix 1 – CT-images of PMO 236.400. The tooth is shown in labial- and mesio-distal view with lines (orange) showing the four different sections (A, B, D and D). CT-sections are not in scale. Abbreviations: en, Enameloid; os, Osteodentine; or, Orthodentine.

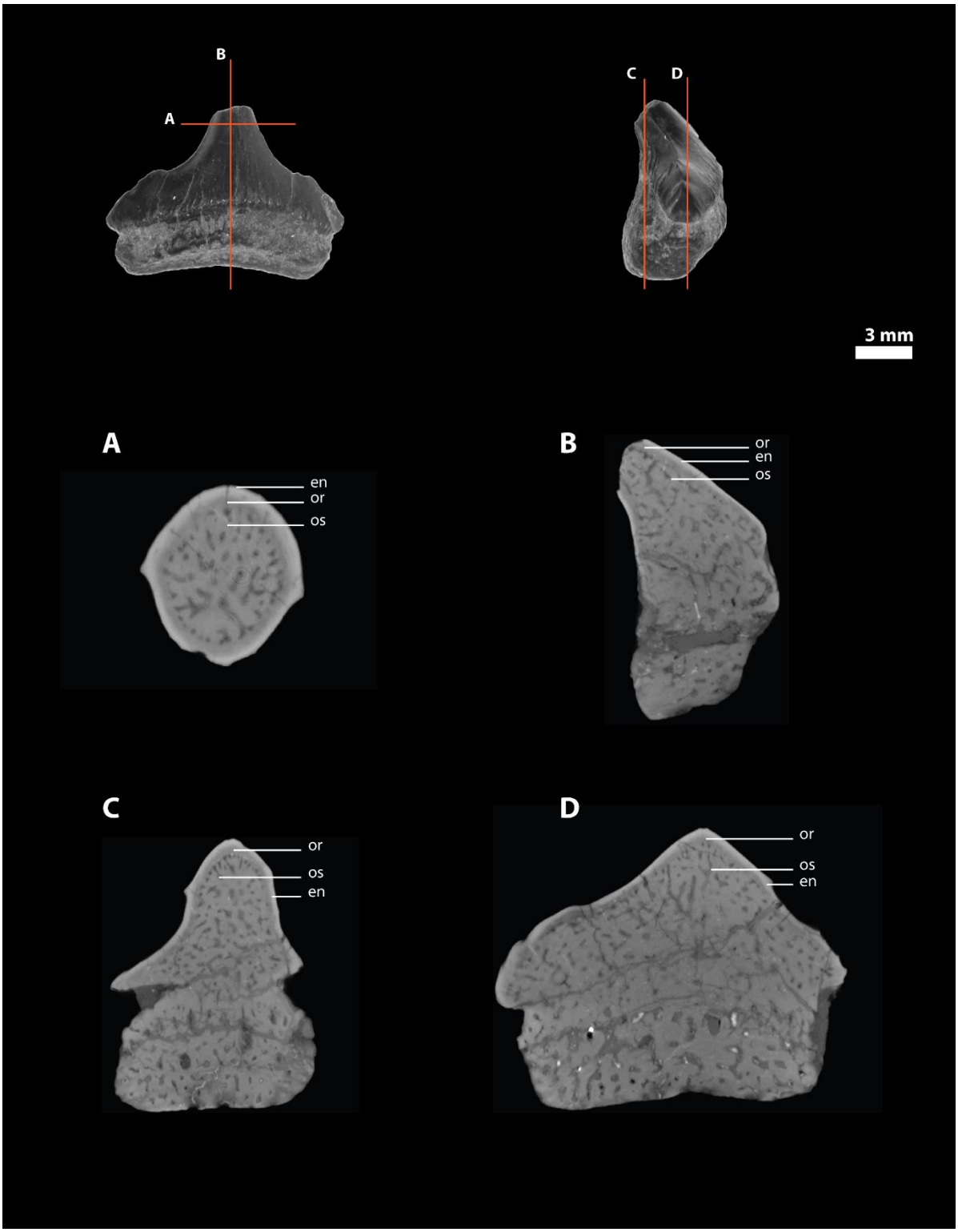

Appendix 2 – CT-images of PMO 241.385. The tooth is shown in labial- and mesio-distal view with lines (orange) showing the five different sections (A, B, C, D and E). CT-sections are not in scale. Abbreviations: d, Dentine; en, Enameloid; OC, Occlusal crest; SSR, Secondary serration; TCR, Transverse crest.

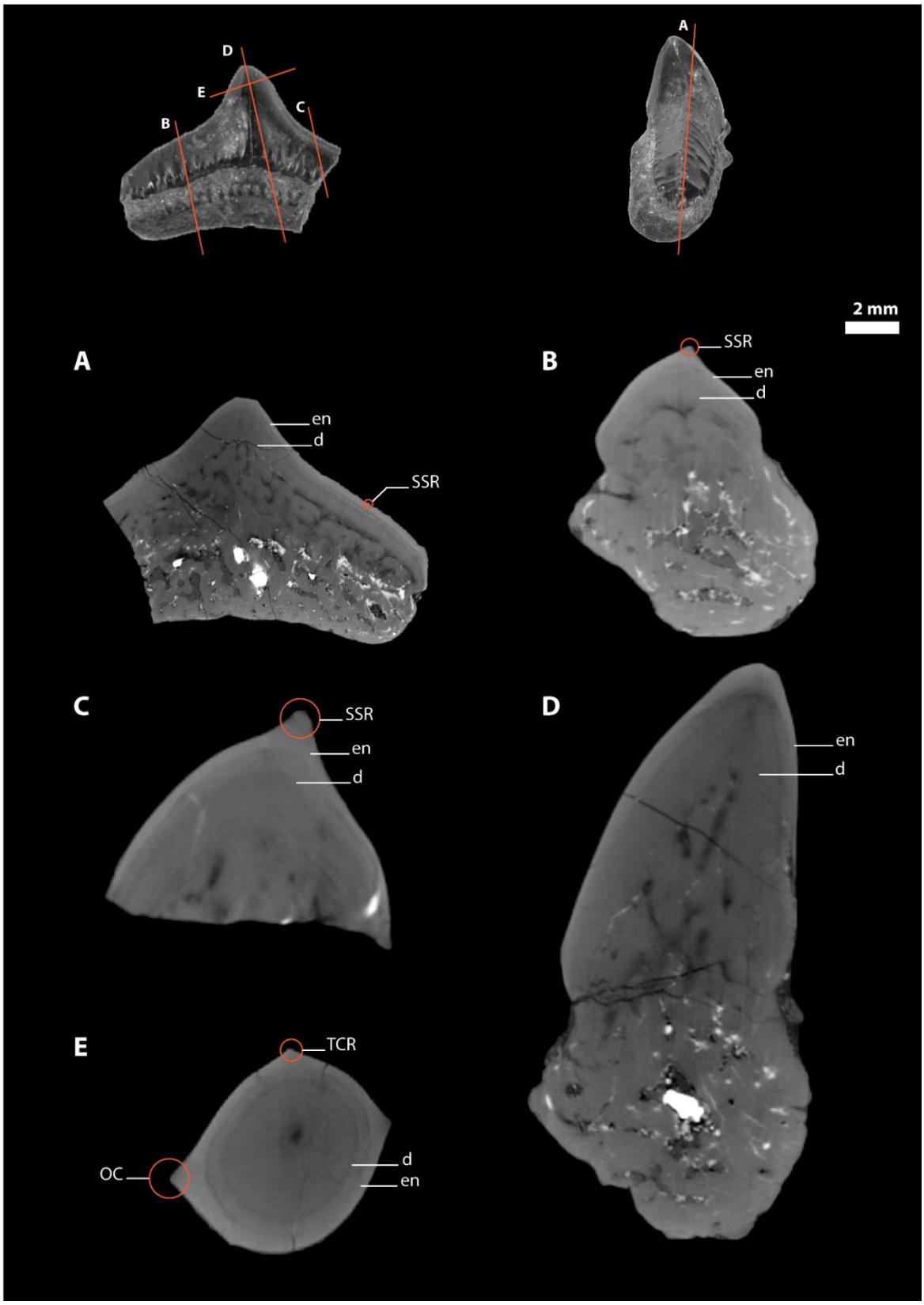

Appendix 3 – CT-images of PMO 241.470. The tooth is shown in labial- and mesio-distal view with lines (orange) showing the four different sections (A, B, C and D). CT-sections are not in scale. Abbreviations: d, Dentine; en, Enameloid; PSR, Primary serration; SSR, Secondary serration.